Segmental Aortic Stiffening Contributes to Experimental Abdominal Aortic Aneurysm Development

Uwe Raaz, MD; Alexander M. Zöllner, MS; Isabel N. Schellinger; Ryuji Toh, MD, PhD; Futoshi Nakagami, MD, PhD; Moritz Brandt, MD; Fabian C. Emrich, MD; Yosuke Kayama, MD, PhD; Suzanne Eken, MD; Matti Adam, MD; Lars Maegdefessel, MD, PhD; Thomas Hertel, MD; Alicia Deng; Ann Jagger, PhD; Michael Buerke, MD; Ronald L. Dalman, MD; Joshua M. Spin, MD, PhD; Ellen Kuhl, PhD; Philip S. Tsao, PhD

Background—Stiffening of the aortic wall is a phenomenon consistently observed in age and in abdominal aortic aneurysm (AAA). However, its role in AAA pathophysiology is largely undefined.

Methods and Results—Using an established murine elastase-induced AAA model, we demonstrate that segmental aortic stiffening precedes aneurysm growth. Finite-element analysis reveals that early stiffening of the aneurysm-prone aortic segment leads to axial (longitudinal) wall stress generated by cyclic (systolic) tethering of adjacent, more compliant wall segments. Interventional stiffening of AAA-adjacent aortic segments (via external application of surgical adhesive) significantly reduces aneurysm growth. These changes correlate with the reduced segmental stiffness of the AAA-prone aorta (attributable to equalized stiffness in adjacent segments), reduced axial wall stress, decreased production of reactive oxygen species, attenuated elastin breakdown, and decreased expression of inflammatory cytokines and macrophage infiltration, and attenuated apoptosis within the aortic wall, as well. Cyclic pressurization of segmentally stiffened aortic segments ex vivo increases the expression of genes related to inflammation and extracellular matrix remodeling. Finally, human ultrasound studies reveal that aging, a significant AAA risk factor, is accompanied by segmental infrarenal aortic stiffening.

Conclusions—The present study introduces the novel concept of segmental aortic stiffening as an early pathomechanism generating aortic wall stress and triggering aneurysmal growth, thereby delineating potential underlying molecular mechanisms and therapeutic targets. In addition, monitoring segmental aortic stiffening may aid the identification of patients at risk for AAA. **(*Circulation*. 2015;131:1783-1795. DOI: 10.1161/CIRCULATIONAHA.114.012377.)**

Key Words: aneurysm ■ aorta ■ arterial stiffness ■ stress, mechanical ■ vascular remodeling

Abdominal aortic aneurysm (AAA) carries a high mortality in the case of rupture.[1] Current therapies are limited to open surgical or interventional stent-based exclusion of the aneurysmal sac from the circulation to prevent rupture. However, these treatment options are generally reserved for larger aneurysms (typically AAA diameter >5.5 cm), and there is no effective therapy targeting the evolution of small aneurysms. This lack of treatment options partly derives from an insufficient understanding of early AAA pathogenesis.

Editorial see p 1745
Clinical Perspective on p 1795

Recent evidence suggests that AAA formation is not simply attributable to aortic wall degeneration, resulting in passive lumen dilation, but to active, dynamic remodeling. The latter involves transmural inflammation, extracellular matrix (ECM) alterations including elastin fragmentation and (compensatory) collagen deposition, vascular smooth muscle cell (VSMC) apoptosis, and oxidative stress.[1–4]

From a pathomechanistic point of view it is essential not only to characterize the particular cellular and molecular alterations involved in AAA formation, but also to identify early triggers of remodeling. In that respect, mechanical wall stress is an intriguing candidate. Biomechanical stress

Received April 3, 2014; accepted March 5, 2015.

From Division of Cardiovascular Medicine, Stanford University School of Medicine, CA (U.R., I.N.S., R.T., F.N., Y.K., M.A., A.D., A.J., J.MS., P.S.T.); Cardiovascular Institute, Stanford University School of Medicine, CA (U.R., A.M.Z., F.N., M.B., F.C.E., Y.K., M.A., R.L.D., J.M.S., P.S.T.); VA Palo Alto Health Care System, CA (U.R., I.N.S., Y.K., M.A., A.D., A.J., J.M.S., P.S.T.); Department of Mechanical Engineering, Stanford University School of Medicine, CA (A.M.Z., E.K.); Department of Cardiothoracic Surgery, Stanford University School of Medicine, CA (F.C.E., E.K.); Department of Medicine, Karolinska Institute, Stockholm, Sweden (S.E., L.M.); Center for Vascular Medicine, Zwickau, Germany (T.H.); Division of Cardiovascular Medicine and Intensive Care Medicine, Saint Mary's Hospital, Siegen, Germany (M.B.); Division of Vascular Surgery, Stanford University School of Medicine, CA (R.L.D.); and Department of Bioengineering, Stanford University School of Medicine, CA (E.K.).

The online-only Data Supplement is available with this article at http://circ.ahajournals.org/lookup/suppl/doi:10.1161/CIRCULATIONAHA.114.012377/-/DC1.

Correspondence to Philip S. Tsao, PhD, VA Palo Alto Health Care System, 3801 Miranda Ave, Building 101 #A2-141, Palo Alto, CA 94304. E-mail ptsao@stanford.edu

(ie, shear stress, circumferential or axial wall stress) may drive adaptive arterial remodeling in response to altered hemodynamics, but also may induce inflammation and ECM remodeling, and VSMC apoptosis, as well, in vascular disease.[4,5]

AAA growth is accompanied by increasing wall stress.[6,7] Although wall stress attributable to the vessel's expanding geometry significantly contributes to the eventual rupture of the mature AAA, it might appear that wall stress would be unrelated to the pathophysiology in early, preaneurysmal stages, when aortic size has not yet overtly changed. However, enhanced wall stress may still occur owing to early aortic biomechanical alterations (ie, aortic stiffening).

AAA formation is associated with a substantially increased wall stiffness.[8,9] Additionally, pronounced stiffening of the abdominal aorta occurs with aging, a major risk factor for AAA.[10] We hypothesize that the existence of a stiff aortic segment adjacent to a more compliant aorta (ie, segmental aortic stiffness [SAS]) generates axial wall stress attributable to nonuniform systolic wall deformations, thereby modulating early aneurysm pathobiology (Figure 1).

Materials and Methods

Details are described in the online-only Data Supplement.

Porcine Pancreatic Elastase Infusion Model

The porcine pancreatic elastase (PPE) infusion model to induce AAA in 10-week-old male C57BL/6J mice was performed as previously described.[11] In brief, after placing temporary ligatures around the proximal and distal aorta, an aortotomy was created at the bifurcation and an insertion catheter was used to perfuse the aorta for 5 minutes with saline containing PPE (1.5 U/mL; Sigma Aldrich).

Glue Treatment of the PPE-Adjacent Aortic Segments

To locally enhance aortic mechanical stiffness, a surgical adhesive (BioGlue, CryoLife, Atlanta) was applied to the segments adjacent to the PPE-treated aorta directly after completion of the PPE treatment. Complete polymerization of the 2-component glue (albumin/glutaraldehyde) occurred within seconds. Care was taken to avoid the PPE-treated segment (Figure II in the online-only Data Supplement). For sham-treatment groups, only 1 component of BioGlue was applied.

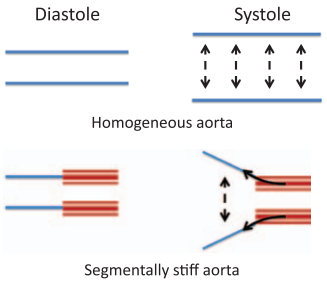

Figure 1. Concept of segmental aortic stiffening (SAS) generating axial wall stress during systolic aortic expansion. In contrast to a homogenous expandable vessel a segmentally stiff aorta (stiff segment in red) is subjected to axially tethering forces (solid arrows) during the systolic circumferential expansion of the adjacent compliant wall segments.

Mouse Ultrasound Studies

Systolic diameter (D_s) and diastolic diameter (D_d) were quantified in the PPE-treated segment, and in the adjacent untreated segments, as well, by using M-mode ultrasound. Circumferential cyclic strain ε was calculated as $\varepsilon=(D_s-D_d)/D_d\times100\%$. SAS was defined as a relative index to quantify the stiffness of the PPE-treated segment in relation to the adjacent aorta, calculated as $SAS=\varepsilon_{adjacent\ aorta}/\varepsilon_{PPEsegment}$. The strain values for adjacent aorta ($\varepsilon_{adjacent\ aorta}$) represent an average strain calculated from the adjacent segments proximal and distal to the PPE-treated segment. For shear-stress calculations, blood flow was assessed as previously described.[12]

Human Ultrasound Studies

Nineteen male volunteers of different ages (youngest age, 36; oldest age, 71; mean age, 51.9 years) were included in the study. Exclusion criteria were cardiovascular diseases (in particular AAA), diabetes mellitus, and history of smoking. M-mode images tracking the anterior and posterior aortic wall motion were recorded at predefined locations (suprarenal, midinfrarenal, and proximal to the aortic bifurcation).

Systolic diameter and diastolic diameter were quantified in the suprarenal, midinfrarenal, and bifurcational segment of the abdominal aorta to calculate cyclic strain and SAS.

Finite-Element Analysis

Finite-element analyses (FEA) of the mouse aorta were performed by using the commercial finite-element software package ABAQUS. The artery was modeled as a 2.0-mm-long axisymmetric tube with outer diameter D_a=0.9 mm and arterial wall thickness t=0.075 mm. The intima, media, and adventitia were summarized in a single homogeneous layer modeled by using an isotropic Neo-Hookean strain energy function with a shear modulus of 300 kPa. Stiffness of the stiff segment (l=1.0 mm) was modified as indicated.

RNA Quantification

Total aortic RNA was isolated and processed for real-time quantitative reverse transcription polymerase chain reaction by using standard protocols and methods.

Laser Capture Microdissection

Laser capture microdissection was performed as previously described.[13] F4/80-stained macrophages were microdissected from frozen aortic cross-sections (7 μm) by using a PALM MicroBeam System (Zeiss). RNA was subsequently processed for real-time quantitative reverse transcription polymerase chain reaction with the use of the Single Cell-to-CT Kit (Ambion).

Histology, Immunofluorescence, In Situ Dihydroethidium Staining, and In Situ Hybridization

Standardized protocols were used, with details available in the online-only Data Supplement.

Ex Vivo Aortic Mechanical Stimulation

Abdominal aortae were explanted, cannulated, and mounted in the heated vessel chamber of a pressure arteriograph system (model 110P, Danish Myotechnology, Copenhagen, Denmark) and stretched to in vivo length. The aorta was then subjected to an automated pressure protocol, cyclically alternating between 80 mm Hg and 120 mm Hg with a frequency of 4/min for 1 hour. To stiffen/restrain either the complete aorta or just the central segment (to simulate segmental stiffening), a silicone cuff (SILASTIC Laboratory Tubing; inner diameter, 0.51 mm; Dow Corning) was placed around the aorta (Figure I in the online-only Data Supplement). After the conclusion of the experiment, the aorta was removed from the cannula and processed for RNA isolation.

Statistics

Data are presented as mean±standard error of the mean. For comparison of 2 groups, Mann-Whitney test was performed; multiple groups (≥3 groups) comparison was accomplished by Kruskal-Wallis test with the Dunn post test. Ultrasound data comparing 2 groups/treatments over time were analyzed by permutation *F* test based on 2-way repeated-measures analysis of variance. For each treatment assignment, we performed a repeated-measures analysis of variance and derived a null distribution of the *P* value for treatment effect. The *P* value from the permutation test was then established as the percentage of the null *P* values less than the *P* value from the real data. To compare ultrasound parameters within 1 treatment group over time, the Friedman test was used. For correlation analysis of animal ultrasound data, Spearman correlation was used. For correlation analyses of human ultrasound data, Pearson correlation was used after passing D'Agostino-Pearson omnibus normality test. A value of $P \leq 0.05$ (2-sided) was considered statistically significant.

Study Approval

All animal protocols were approved by the Administrative Panel on Laboratory Animal Care at Stanford University (http://labanimals.stanford.edu/) and followed the National Institutes of Health and US Department of Agriculture Guidelines for Care and Use of Animals in Research.

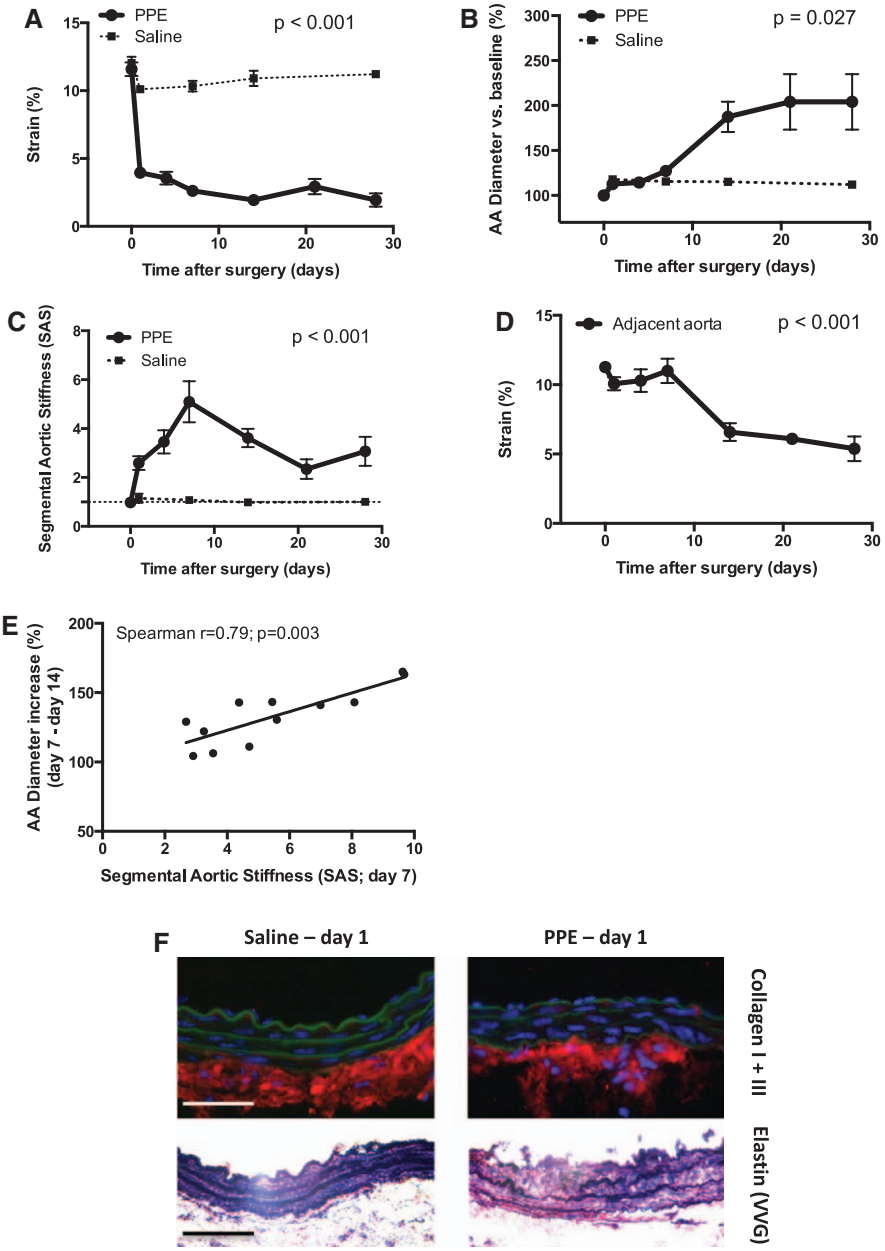

Figure 2. Analysis of segmental aortic stiffening and aneurysm progression in the PPE model. **A**, Temporal development of circumferential cyclic strain of PPE- and saline-treated segments. **B**, Diameter development of the PPE- and saline-treated segments (% vs baseline [d0]). **C**, Temporal analysis of segmental aortic stiffening (SAS) of the PPE- or saline-treated segment relative to the adjacent abdominal aorta. **D**, Temporal analysis of the circumferential cyclic strain of the adjacent aorta. **E**, Correlation between the SAS at d7 and the consecutive diameter increase of the PPE-treated segment in the following 7 days. **F**, **Top**, Representative immunofluorescence staining for collagen I + III (red) with green autofluorescence of elastin lamellae. **Bottom**, Modified elastin Verhoeff's Van Gieson (VVG) staining. Data are mean±SEM. n=5 to 13 for each condition/time point; *P* values denote differences between PPE and saline groups by the permutation *F* test (**A** through **C**), aortic strain differences in PPE-treated animals over time by the Friedman test (**D**), or significance level of Spearman correlation (**E**). AA indicates abdominal aorta; PPE, porcine pancreatic elastase; and SEM, standard error of the mean.

Results

Aortic Stiffening Precedes Aneurysmal Dilation in Experimental AAA

We investigated the temporal relationship between aortic biomechanical alterations and aneurysmal dilation in the PPE-infusion model of murine AAA. Circumferential cyclic aortic strain (as a measure of vascular stiffness) and aortic diameter were monitored over time in the PPE-treated segment and saline-perfused controls via M-mode ultrasound (Figure 2A and 2B).

Although native abdominal aortae exhibited a baseline cyclic strain of ≈12%, PPE infusion rapidly induced a substantial strain reduction of >50% in the treated segment at day 1 (d1) followed by further declines until d14, after which it remained stable until d28. In contrast, saline infusion only resulted in a minor strain reduction in the corresponding segment (Figure 2A).

The aortic diameter, however, displayed insignificant enlargement up to d7 post-PPE and postsaline. The PPE-treated segment then dilated markedly between d7 and d14. Afterward the aortic diameter remained relatively stable up to d28 (Figure 2B).

Investigating possible mechanisms for the rapid stiffening of the PPE-treated segments, we found remarkable elastin fragmentation, whereas profibrotic responses were only moderate (Figure 2F).

SAS Generates Axial Wall Stress in the AAA-Prone Segment

Having identified rapid early mechanical stiffening of the aneurysm-prone segment (ie, reduced cyclic strain), we sought to investigate its role in aneurysm development. We hypothesized that SAS (defined as enhanced stiffness of the aneurysm-prone segment relative to the adjacent aorta) would generate adverse wall stress during cyclic deformation of the aortic wall, eventually resulting in AAA formation. We therefore performed *in silico* wall stress analysis by using a finite-element model.

With the use of a simplified approach, the infrarenal mouse aorta was modeled as a cylindrical tube. To examine the effects of segmental stiffening we simulated a pressure of 130 mm Hg (approximating systolic blood pressure) and introduced a segment of increasing stiffness adjacent to a nonstiff segment. We found that increasing segmental stiffness progressively induced axial stress in the stiff segment extending from the segmental interface (Figure 3A).

Because hypertension represents a risk factor for AAA, we explored the impact of high blood pressure levels on axial wall stress by pressurizing our FEA model with a fixed stiffness of the stiff segment up to 180 mm Hg. This simulation revealed that high blood pressure augmented segmental stiffness–based wall stresses (Figure 3B).

Taken together, these data suggest that SAS generates substantial axial wall stresses that also are susceptible to a hypertensive environment.

SAS Correlates With Experimental Aneurysm Progression

To further investigate the significance of SAS as an inducer of aneurysm growth, we performed temporal analysis of SAS in vivo and correlated it to aneurysm growth in the PPE model. We found a continuous increase in SAS after aneurysm induction, peaking at d7, which was attributable to increasing stiffness of the PPE-treated segment (5-fold higher than adjacent

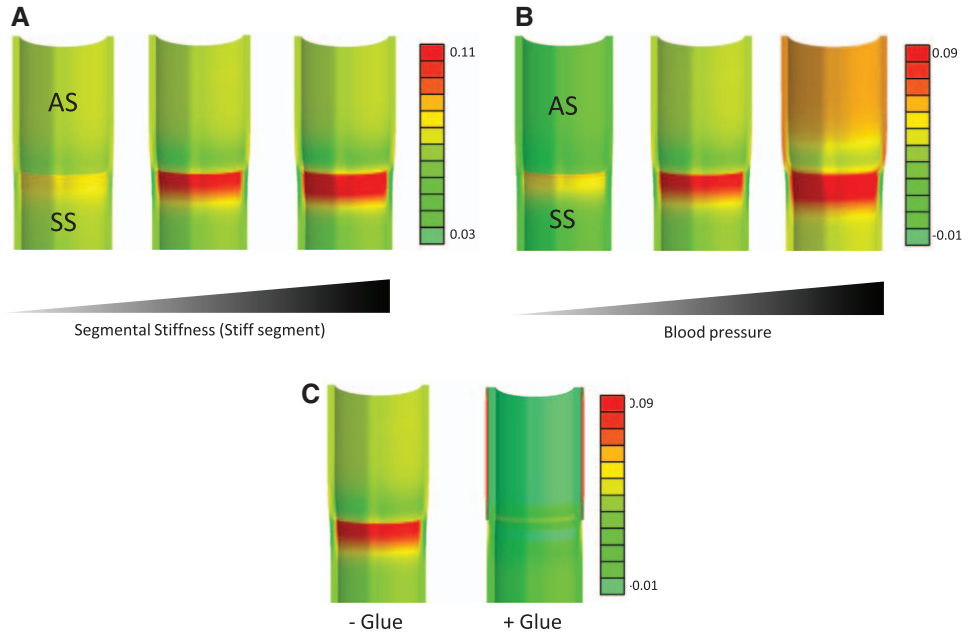

Figure 3. Finite-elements analysis (FEA)–based axial stress analysis of segmental aortic stiffening. A simplified model of the murine infrarenal aorta was subjected to various mechanical conditions, and the resulting axial (longitudinal) stress (N/mm^2) was depicted. **A**, The stiffness of the stiff aortic segment (SS) was increased (Shear moduli, 500 kPa left vessel, 1100 kPa middle vessel, 1700 kPa right vessel) to demonstrate the impact of segmental stiffness on axial stress generation. **B**, The intraluminal pressure was increased (left vessel, 80 mm Hg; middle vessel, 130 mm Hg; right vessel, 180 mm Hg) to visualize the influence of blood pressure on axial stresses in a segmentally stiff aorta. **C**, A segmentally stiff aorta (**Left**) is subjected to external stiffening of the adjacent compliant segments (simulating glue treatment; **Right**) to demonstrate axial stress reduction and homogenization induced by the intervention. AS indicates adjacent, nonstiff segment.

aorta; Figure 2C and 2D). Of note, the SAS peak coincided with the onset of aneurysm expansion. Moreover, the magnitude of SAS at d7 correlated with subsequent aortic enlargement between d7 and d14 (Figure 2E).

After d7 SAS declined as a result of progressive stiffening of the adjacent aortic segments (Figure 2C and 2D), which was accompanied by decelerating aortic diameter enlargement (Figure 2B). Saline-infused controls did not exhibit significantly enhanced SAS at any point during the entire observation period (Figure 2C).

Profibrotic Mechanisms Accompany Stiffening of AAA-Adjacent Segments, Thereby Reducing SAS

Having detected decreased SAS at d14 owing to stiffening in the AAA-adjacent aorta, we investigated the underlying molecular mechanisms.

Medial collagen deposition, a known determinant of arterial stiffness, was remarkably enhanced in AAA-adjacent segments at d14 after aneurysm induction (in comparison with d7; Figure 4D). Expression of the collagen genes *Col1a1* and *Col3a1* was increased in the adjacent segments in comparison with the AAA segment itself at d7 (Figure 4A), preceding the histological alterations. In line with this observation, miR-29b, previously shown to be an epigenetic negative regulator of collagen expression in AAA, was similarly downregulated at d7 (Figure 4B). More specifically, in situ hybridization indicated marked miR-29b downregulation within the aortic media (Figure 4C).

In contrast to the marked profibrotic changes, elastin architecture appeared unaffected in the AAA-adjacent aorta (Figure 4D).

Interventional Reduction of Segmental Stiffness Reduces Wall Stress and Aneurysm Progression

To investigate the potential causative role of SAS as a mechanism driving AAA development, we focally stiffened the adjacent aorta next to the PPE-treated segment by periaortic

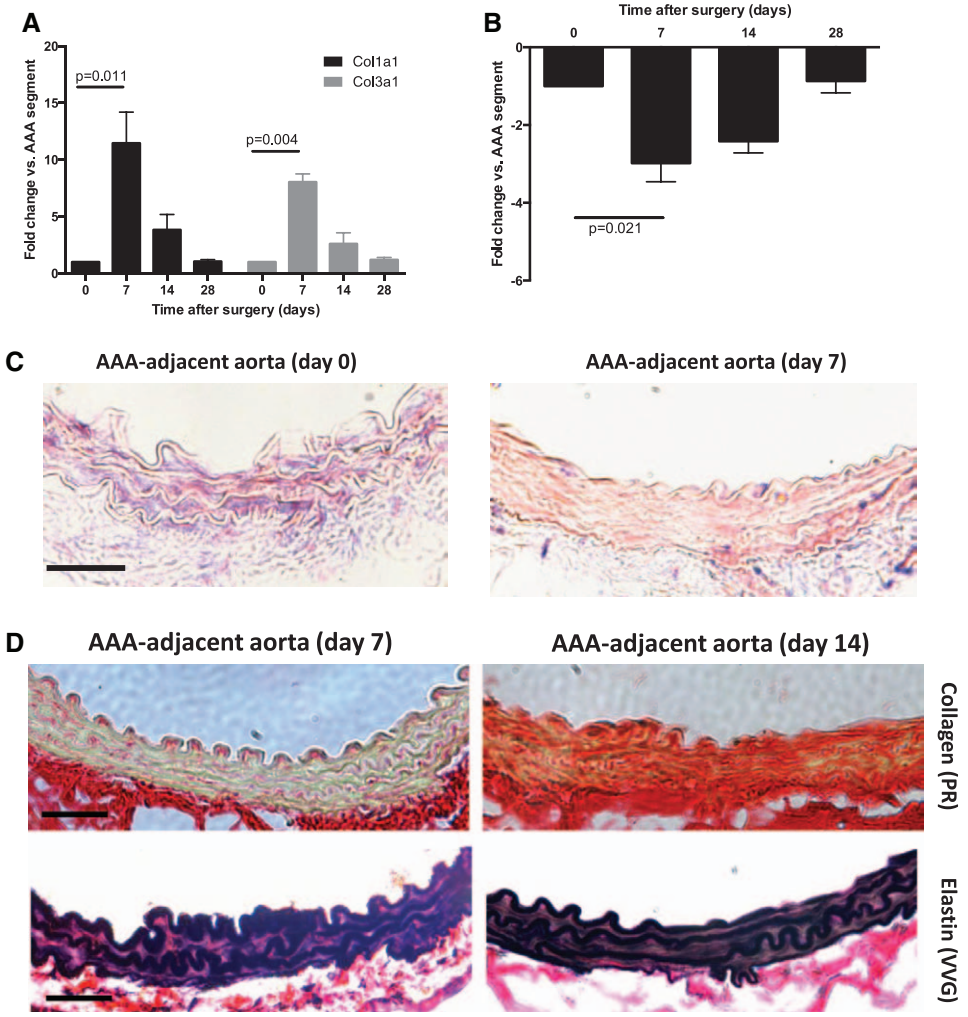

Figure 4. Stiffening mechanisms of the AAA-adjacent aorta. **A**, Temporal analysis of the *Col1a1* and *Col3a1* gene expression in the AAA-adjacent aorta in comparison with the AAA (PPE-treated) segment. **B**, Temporal analysis of miR-29b expression in the AAA-adjacent aorta in comparison with the AAA (PPE-treated) segment. **C**, In situ hybridization for miR-29b (purple-blue dye) and red nuclear counterstain in the AAA-adjacent aortic segments (original magnification ×400; scale bar, 50 μm). **D**, Representative images of the aortic wall taken from AAA-adjacent aortic segments 7 days or 14 days after PPE treatment stained with Picrosirius Red (**Top:** red, collagen; yellow, muscle) and elastin VVG staining (**Bottom**). Original magnification ×400; scale bar, 50 μm. n=5 for each time point; *P* values denote differences between expression levels by Kruskal-Wallis test with Dunn post test. AAA indicates abdominal aortic aneurysm; PPE, porcine pancreatic elastase; and VVG, Verhoeff's Van Gieson.

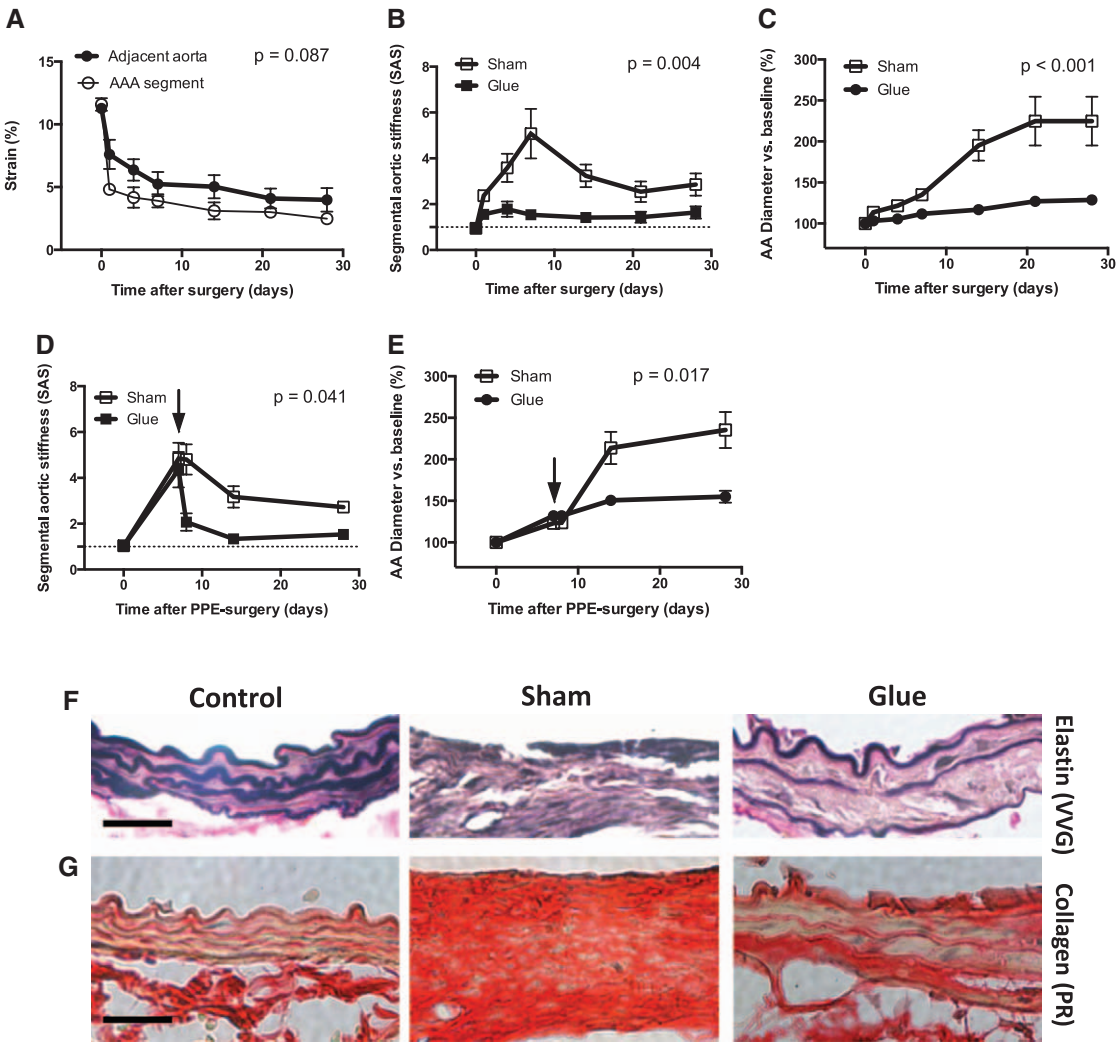

Figure 5. Effects of glue treatment on segmental aortic stiffening (SAS) and aneurysm progression. **A**, Temporal analysis of the circumferential cyclic strain of the glue-treated adjacent aorta (bold line) in relation to the PPE-treated segment (thin line). **B**, Temporal analysis of SAS in glue-treated aortas in comparison with sham glue–treated conditions. **C**, Diameter development of the PPE-treated segment in glue-treated vs sham glue–treated conditions. Temporal development of SAS (**D**) and aortic diameter (**E**) following delayed glue or sham treatment 7 days after PPE surgery (arrows). Representative elastin VVG staining (**F**) or Picrosirius Red staining (**G**) of the aortic wall taken from native abdominal aortas (control) or PPE-treated segments (d14) after additional treatment of the adjacent aorta with glue or sham glue (original magnification ×400; scale bars, 50 μm). VVG staining was used to depict the integrity of the medial elastin lamellae. Picrosirius Red staining aided the visualization of the aortic wall architecture and collagen remodeling. n=7 for each time point; *P* values denote differences between aortic segments (**A**) or treatment groups (**B** through **E**) by permutation *F* test. AA indicates abdominal aorta; AAA abdominal aortic aneurysm; d, day; PPE, porcine pancreatic elastase; PR, Picrosirius Red; and VVG, Verhoeff's Van Gieson.

application of BioGlue, a surgical adhesive with a relatively high material stiffness (Figure II in the online-only Data Supplement). Glue application induced rapid and sustained stiffening of the adjacent aortic segments (Figure 5A), resulting in near-equalization of stiffness between the PPE-treated segment and the glue-treated adjacent segments. This was reflected in a significant reduction of SAS in comparison with sham glue–treated controls (Figure 5B).

To exclude the possibility that aortic constriction attributable to segmental glue treatment might lead to alterations of the downstream aortic flow and fluid shear stress, thereby affecting aneurysm formation, we monitored the aortic diameter of the glue-treated segment and the downstream flow profile, as well. We detected neither luminal narrowing (data not shown) nor elevated flow shear stress levels (Figure III in the online-only Data Supplement). Glue treatment of the adjacent aorta did not cause perturbations of its elastin architecture nor an enhanced fibrotic response (Figure IV in the online-only Data Supplement), suggesting that direct mechanical interaction with the aortic wall caused the stiffening effect.

Further, our finite-element model demonstrated that stiffness equalization between all segments (ie, reduction of SAS) resulted in decreased and homogenized axial stress (Figure 3C).

Finally, comparing aortic diameter between glue-treated and sham glue–treated animals, we found that PPE-induced aortic expansion was significantly reduced when adjacent segments were immobilized by glue application. The expected rapid diameter increase between d7 and d14 was suppressed (Figure 5C).

To further test the efficiency of delayed glue treatment on aneurysm progression, we performed additional experiments with glue intervention at d7 post-PPE, when there already is a small dilation combined with a high segmental stiffness (Figure 5D and 5E). As a result, we found that delayed glue stiffening of the AAA-adjacent aorta also significantly reduces SAS and thereby represses the consecutive aneurysmal diameter progression in comparison with sham glue–treated animals (Figure 5D and 5E).

Reduction of Segmental Stiffness Modulates Critical Features of AAA Pathobiology

Because AAA formation is accompanied by extensive ECM remodeling, we performed histological analyses of the aneurysm wall, focusing on elastin and collagen architecture. Extensive destruction of elastin fibers, a hallmark of aneurysm pathology, was present in sham glue–treated mice on d14 after PPE infusion (Figure 5F). Further, Picrosirius Red staining revealed disturbed wall architecture with general wall thickening, loss of layered structure, and diffuse collagen enrichment (Figure 5G). In contrast, elastin structure and wall layering were better preserved in the glue-treated group, whereas collagen accumulation appeared less prominent (Figure 5F and 5G).

AAA pathology includes enhanced reactive oxygen species (ROS) generation, vascular inflammation, VSMC apoptosis, and enhanced matrix metalloproteinase (MMP) activity. To assess the impact of SAS modulations on these end points, we analyzed the PPE-treated aorta at d7, which marks the peak of segmental stiffening but precedes the prominent diameter increase between d7 and d14.

We performed in situ dihydroethidium fluorescence to monitor ROS generation. PPE-treated segments exhibited enhanced nuclear fluorescence in comparison with native controls, whereas glue treatment resulted in a significant decrease in ROS production (Figure 6A and 6B).

Inflammation was quantified by aortic macrophage infiltration and cytokine analysis. Extensive macrophage infiltration of the aortic wall was present 7 days after aneurysm induction as assessed by immunofluorescence (Figure 6C through 6E), accompanied by enhanced aortic gene expression of *Il6*, *Ccl2*, and *Il1b* (Figure 6G). Immunofluorescence additionally revealed macrophage colocalization with each of these cytokines (Figure V in the online-only Data Supplement). Glue treatment reduced macrophage infiltration, and cytokine expression, as well (Figure 6C through 6E).

To further delineate the role of macrophages in vascular cytokine production, we analyzed gene expression profiles of macrophages directly isolated from the PPE-aneurysm sections via laser capture microdissection. To this end, we microdissected macrophages (positive F4/80 staining) from the aortic wall and confirmed macrophage transcript enrichment by enhanced *Emr1* expression (encoding for F4/80 protein) in comparison with randomly captured F4/80-negative cells (Figure VI in the online-only Data Supplement). Macrophages isolated from sham glue treatment exhibited significantly higher expression of *Il1b*, *Il6*, and *Ccl2* than those from glue-stiffened samples (Figure 6H).

Assessing apoptosis, we detected enhanced capase-3 activity in the intimal and medial layer of PPE-treated aortic wall, which was reduced in the glue-treated group (Figure 6F).

MMP2 and MMP9 are essential for matrix macromolecule degradation in AAA. In accordance with the substantial elastin breakdown found in PPE-treated segments, both *Mmp2* and *Mmp9* were significantly upregulated. Glue stabilization of the adjacent aortic segments, which prevented extensive elastin breakdown and collagen remodeling, minimized Mmp expression (Figure 6I). Additionally, this intervention reduced the enhancement of *Col1a1* and *Col3a1* expression after aneurysm induction (Figure 6J).

Ex Vivo SAS Induces Upregulation of AAA-Related Genes

We examined the mechanism of SAS as a driver of AAA pathogenesis by validating our in vivo findings ex vivo. We explanted murine abdominal aortic segments and mounted them onto a pressure myograph system. Aortae were then subjected to physiological pressure levels, cyclically alternating between 80 mm Hg and 120 mm Hg. To simulate aortic stiffening, the systolic expansion of either the entire aortic segment (complete stiffening) or just the central aortic segment (segmental stiffening) was restrained by an externally applied silicone cuff (Figure 7A, Figure VI in the online-only Data Supplement). After 1 hour of cyclic pressurization, aortic gene expression was analyzed.

Cuffing the entire aortic segment had minimal-to-no effect on the expression of inflammatory cytokines *Il6* and *Ccl2*. Segmental stiffening, in contrast, induced the upregulation of these genes (Figure 7B). Likewise, the expression of metalloproteinases (*Mmp2*, *Mmp9)* and collagen genes (*Col1a1*, *Col3a1*), as well, quantified as indicators of active matrix remodeling, was significantly enhanced only in response to segmental stiffening (Figure 7C and 7D).

The Aging Human Abdominal Aorta Exhibits Segmental Stiffening

To test whether SAS occurs naturally in the human aorta, we assessed the aortic stiffness in 3 distinct locations (suprarenal, midinfrarenal, bifurcational) along the abdominal aortas of 19 male patients ranging in age from 36 to 71 years without evident AAA.

A significant negative correlation was observed between age and aortic cyclic strain in the suprarenal and midinfrarenal, and in the aortic bifurcation segments, as well, suggesting generally enhanced stiffness in the aging abdominal aorta (Figure 8A through 8C).

We also detected important differences between the distinct aortic locations. Although both the midinfrarenal aorta and the bifurcation exhibited age-related strain reduction, the slope of strain reduction was significantly steeper in the bifurcation segment, altering the (relative) SAS between 2 regions. In younger patients, the stiffness between both segments was similar (SAS≈1), but doubled (SAS≈2) by 60 years of age (Figure 8D). These results indicate that, in addition to overall stiffening of the abdominal aorta with age, the human abdominal aorta exhibits age-related segmental stiffening.

Discussion

AAA formation is accompanied by increased stiffness of the aneurysmal vessel segment in comparison with the normal

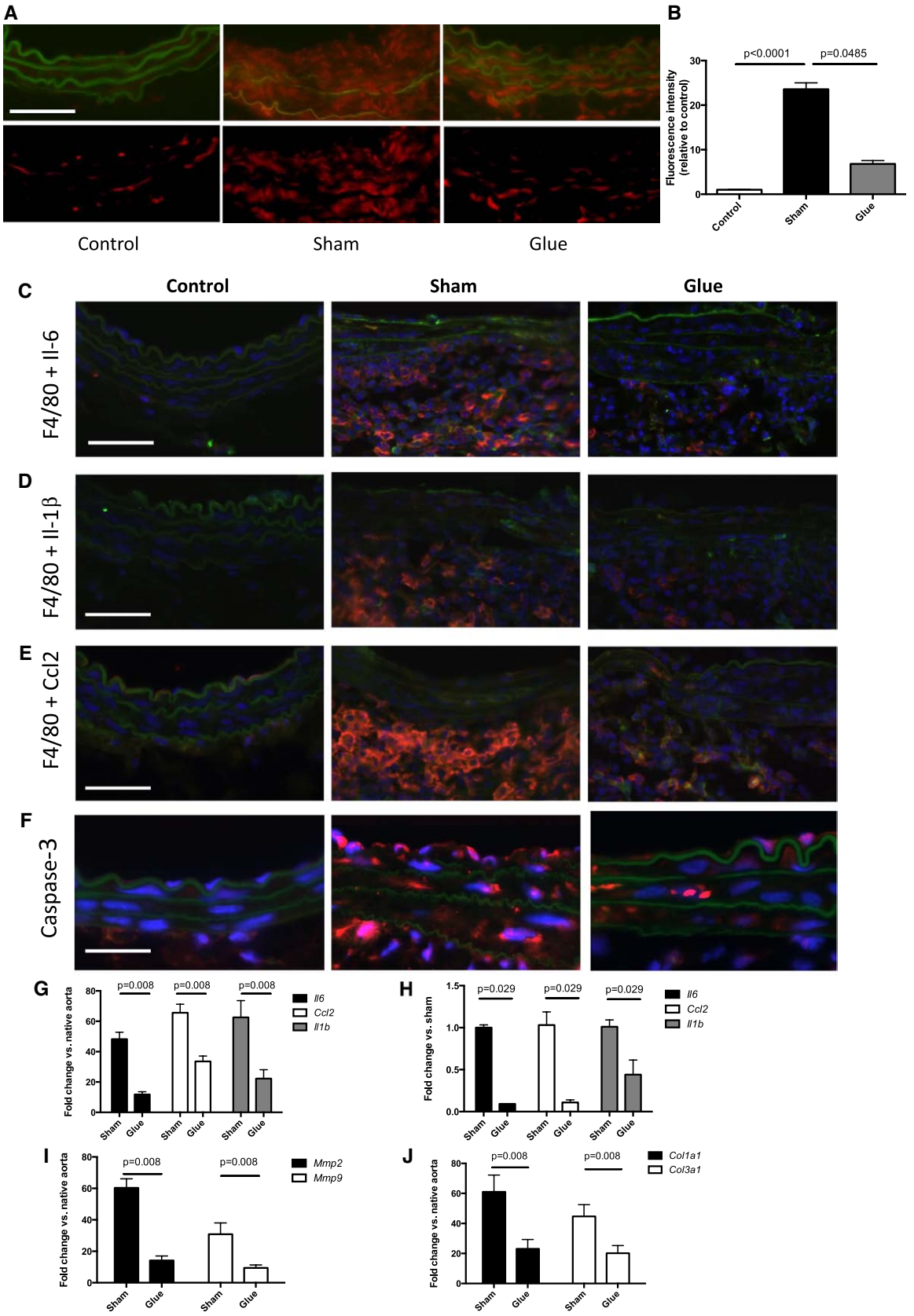

Figure 6. Effects of glue-induced aortic stiffening on ROS generation and parameters of inflammation, apoptosis, and ECM remodeling. **A**, In situ DHE staining of native abdominal aortas (control) or PPE-treated segments after additional treatment of the adjacent aorta with glue or sham glue (d7). ROS production was indicated by red fluorescence. Autofluorescence from elastic lamellae (depicted in green, **Top**) was subtracted (**Bottom**). Original magnification ×400; scale bar, 50 μm. **B**, Average fluorescence was quantified from 3 high-power fields of 3 different aortas per group. **C** through **E**, Representative costaining of macrophages (red F4/80 marker) and the green labeled (*Continued*)

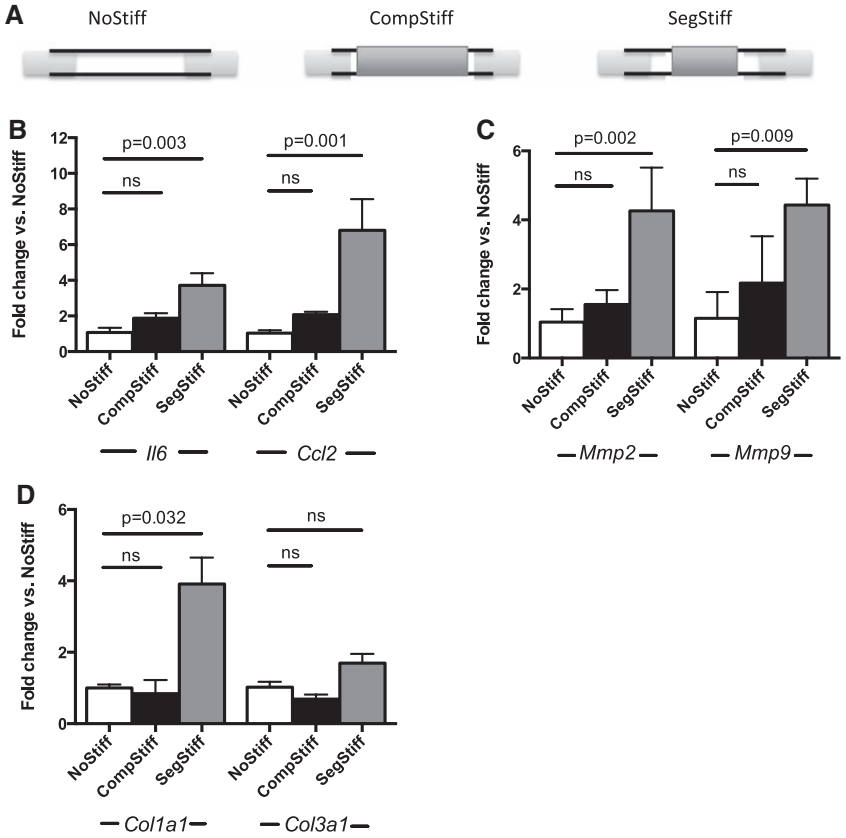

Figure 7. Ex vivo aortic mechanical stimulation. **A**, Scheme of the experimental setup for differential mechanical stimulation of the cannulated aorta. Cyclic strain is imposed on unrestrained/unstiffened aortas (NoStiff), completely restrained aorta (CompStiff), or segmentally restrained aorta (SegStiff). **B** through **D**, Gene expression results after 1 hour of mechanical stimulation in the 3 groups. Depicted is the differential expression of inflammation-related genes *Il6* and *Ccl2* (**B**), matrix metalloproteinases *Mmp2* and *Mmp9* (**C**), and collagen genes *Col1a1* and *Col3a1* (**D**; all vs NoStiff condition). n=5 for each condition; *P* values denote differences between treatment groups by Kruskal-Wallis test with Dunn post test. ns indicates not significant.

aorta.[9,14] Aneurysmal stiffening occurs owing to profound changes in ECM organization, including elastin fragmentation and enhanced adventitial collagen deposition and turnover.[14] The current study was designed to investigate aortic stiffening as a potential factor driving early AAA pathogenesis.

To explore the temporal relationship between aortic stiffening and AAA growth, we used the widely used PPE animal model. Because human AAA typically occurs in the aged aorta, which exhibits progressive elastin degeneration and stiffening,[10,15] we deliberately chose the PPE model as a nondissection type preclinical model of AAA because it not only phenotypically resembles many aspects of the human disease, but it is also initiated by mild destruction of the elastin architecture (although this is achieved enzymatically by PPE perfusion in contrast to fatigue-related elastin fracture in the human situation). Moreover, our previous studies indicated that this model, in particular, appears sensitive to ECM/stiffness–related interventions.[16]

Our data confirm that aortic stiffening precedes aneurysmal dilation.[17] The rapid stiffening that occurred within 1 day after treatment seems to be attributable to early PPE-induced elastin damage (Figure 2F). However, PPE is biologically active for no more than 24 hours after perfusion.[18] Therefore, later structural alterations of the aorta, including the pervasive elastin fragmentation observed after 14 days (Figure 5F), appear to be PPE independent.

Although the observed early and sustained stiffening of the aneurysm-prone aorta may seem counterintuitive, this finding supports aneurysm growth as an active process, as opposed to simple passive dilation. Moreover, segmental stiffening of the abdominal aorta may qualify as a mechanism generating wall stress.

Mechanical stress is a potent inducer of physiological arterial remodeling. High flow–induced shear stress, elevated circumferential stress, and increased axial stress result in increased vessel diameter, wall thickening, and arterial lengthening, respectively, to achieve stress normalization.[5] From a pathogenic point of view, mechanical forces induce a multitude of adverse events contributing to vascular disease, including ROS generation, apoptosis, and inflammation.[4,19–21]

To test the hypothesis that SAS generates wall stress that precedes and triggers early AAA growth, we performed *in silico* stress analysis using a FEA model. Inclusion of a stiff segment in a more compliant aorta generates axial stress under systolic

Figure 6 continued. cytokines IL-6 (**C**), IL-1β (**D**), and Ccl2 (**E**) in native abdominal aortas (control) or PPE-infused segments (d7) after additional treatment of the adjacent aorta with glue or sham glue (original magnification ×400; scale bar, 50 μm). Colocalization results in orange/yellow color. Nuclei are Hoechst stained (blue). **F**, Corresponding immunostaining of activated caspase-3 (red). **G** and **H**, Expression of *Il6*, *Ccl2,* and *Il1b* in the PPE-infused segment (d7) after additional glue or sham-glue treatment of the adjacent aorta, quantified in whole tissue (**G**) and in laser-captured macrophages, as well (**H**). Expression analysis of *Mmp2* and *Mmp9* (**I**) and *Col1a1* and *Col3a1* (**J**), as well (all versus native control) in the PPE-infused segment (d7) after additional glue or sham-glue treatment of the adjacent aorta; *P* values denote differences between treatment groups by Kruskal-Wallis test with Dunn post test (**B**) or Mann-Whitney test (**G** through **J**). d indicates day; DHE, dihydroethidium; ECM, extracellular matrix; IL, interleukin; PPE, porcine pancreatic elastase; and ROS, reactive oxygen species.

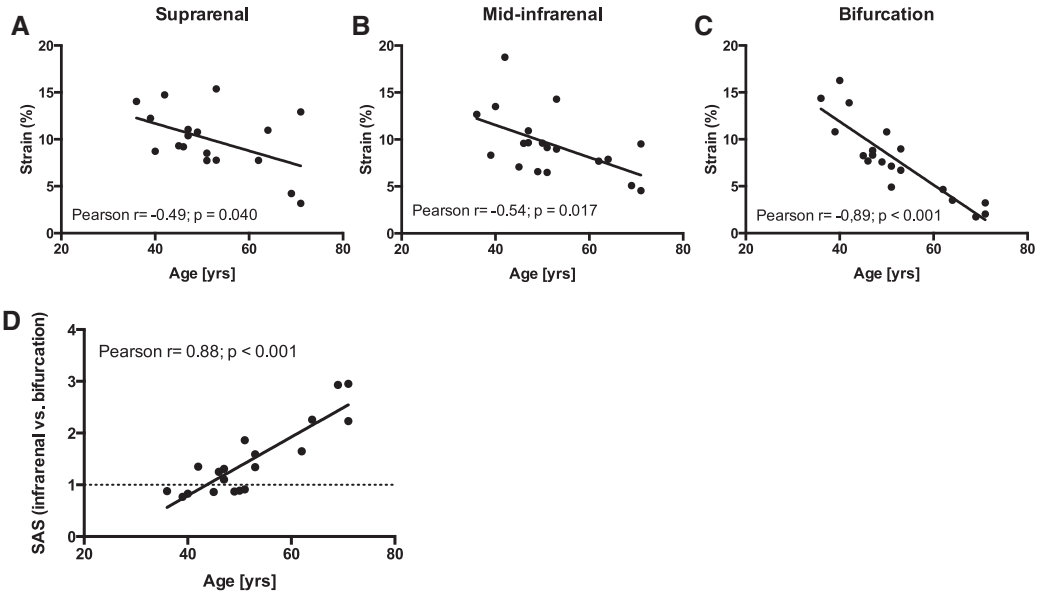

Figure 8. Segmental aortic stiffening in the aging human abdominal aorta. **A** through **C**, Correlation between age and circumferential cyclic strain in the suprarenal (**A**), midinfrarenal (**B**), and bifurcational segment (**C**) of the human abdominal aorta. **D**, Correlation between age and segmental stiffness (SAS, bifurcational segment vs midinfrarenal segment) along the infrarenal abdominal aorta; *P* denotes significance level of Pearson correlation.

pressurization. Axial stress increases with enhanced stiffness gradients between stiff and nonstiff segments (Figure 3A). Hypertension, a known AAA-associated risk factor, further increases axial stress in the setting of SAS (Figure 3B). Of note, this simplified model only takes into account static wall stresses, neglecting dynamic effects that may occur owing to cyclic systolic-diastolic wall deformations.

In our animal model, the peak of SAS at d7 coincided with the onset of accelerated aneurysmal enlargement. Delayed AAA formation until 7 days after PPE treatment is consistent with the initial characterization of this model.[6] The relationship between increasing SAS and subsequent aneurysmal dilation was further strengthened by a positive correlation between the extent of SAS at d7, and aortic diameter enlargement between d7 and d14.

To clarify the pathophysiologic significance of SAS for AAA growth, we selectively applied rapid-hardening biological glue to the aortic segments adjacent to the PPE-injury site, achieving dramatic stiffening of the adjacent aorta, detectable within 1 day after intervention. Subsequently, the relative segmental stiffness of the PPE-treated aorta in comparison with its adjacent segments (ie, SAS) was instantly and permanently reduced. A major finding of this study is that the (glue-induced) reduction in SAS translated into significantly reduced AAA growth. In a more therapeutic context, we additionally found delayed glue application (day 7 after PPE injury) to reduce subsequent AAA progression.

To elucidate the mechanisms of this process we analyzed factors that contribute to AAA, and that are moreover known to be mechanosensitive: ROS generation, inflammation, ECM remodeling, and apoptosis. ROS levels are locally increased in human AAA in comparison with the adjacent nonaneurysmal aorta.[22] ROS may be generated in response to mechanical stress in endothelial cells, and in VSMCs, as well, whereby mechanically activated NADPH oxidases and the mitochondrial electron transport chain seem to be significant sources.[23,24] Mechanically generated ROS may subsequently trigger a variety of cellular responses such as VSMC apoptosis[25] and vascular inflammation.[4] ROS scavengers and NADPH-oxidase inhibition have reduced oxidative stress and aortic macrophage infiltration, and ultimately ameliorated aneurysm growth or decreased aneurysm rupture incidence in various murine AAA models.[26–28] We found decreased ROS generation following glue-mediated reduction of SAS and axial stress.

AAA formation is characterized by inflammatory remodeling of the aortic wall, and vascular inflammatory reactions are sensitive to mechanical stress–induced signaling. For example, mechanical stress–induced proinflammatory mechanisms involve enhanced cytokine production via Ras/Rac1-p38-MAPK-NF-κB (leading to enhanced interleukin-6 expression in VSMC),[20] and enhanced nuclear factor-κB–dependent expression of vascular chemokines and adhesion molecules that facilitate monocyte adhesion to the vascular wall, as well.[21] Interestingly, inflammatory cells such as monocytes/macrophages become mechanosensitive once attached to the vascular ECM.[29] We show that interventional stiffening of the adjacent aorta decreases macrophage infiltration in the aneurysm-prone (PPE-treated) segment and reduces the aortic and macrophage-specific expression of various inflammatory cytokines that are known to be critical for AAA pathogenesis, including Il1b, Il6, and Ccl2.[30–32]

ECM remodeling, with enzymatic breakdown of matrix macromolecules mediated by the metalloproteinases MMP-2 and MMP-9, is another hallmark of AAA. MMP expression is increased in human AAA,[33–35] and knockout of MMP-2 and MMP-9 abolishes experimental AAA formation.[18,36] MMP-2 and MMP-9 are also responsive to mechanical stress attributable to cyclic stretch and enhanced flow.[24,37] More importantly, axial stress induces tissue remodeling and Mmp-2 activation in

a model of longitudinal carotid growth.[38] As expected, *Mmp2* and *Mmp9* were significantly upregulated in PPE-treated aortae (Figure 6I). Reducing SAS, and thereby cyclic axial stress, with glue stiffening reduced expression of both MMPs.

VSMC apoptosis is another critical feature of human and experimental AAA,[39,40] and is susceptible to enhanced mechanical (axial) stress.[38] Signaling mechanisms of mechanical stress-induced VSMC apoptosis include a variety of molecules, such as the endothelin B receptor, integrin-β1-rac-p38-p53 signaling or Bcl-2-associated death factor.[19] We identified enhanced medial layer apoptosis in PPE-treated segments, which was decreased by glue-mediated axial stress reduction.

We further investigated the impact of SAS on inflammation and matrix remodeling ex vivo. Segmental stiffening (induced with an external cuff around the cyclically pressurized aorta) resulted in significant upregulation of *Mmp2* and *Mmp9*, *Col1a1* and *Col3a1,* and *Il6* and *Ccl2*, as well. In contrast to the in vivo situation, where enhanced biaxial stiffness results from alterations of the inherent material properties of the vessel wall, our ex vivo model only simulated circumferential stiffening by external cuffing. Owing to technical limitations, our systolic and diastolic pressure levels alternated with a frequency of 3/min (normal C57BL/6 heart rate, ≈450/min[41]). Nevertheless, the data indicate that cyclic axial mechanical stress may directly control genes governing inflammation and matrix remodeling.

We observed stiffening of the aneurysm-adjacent aorta at d14 after PPE induction, with subsequent reduction of aneurysm growth rate. This might represent an endogenous compensatory mechanism to reduce SAS and contain AAA progression. The stiffening process was paralleled by an enhanced fibrotic response in the AAA-adjacent segments' media, including upregulated collagen expression. A previous study showed that microRNA (miR)-29b is a repressor of collagen expression in AAA.[16] We identified analogous miR-29b downregulation in the (VSMC-dominated) media of the AAA-adjacent aortic segments, consistent with miR-29b–modulated VSMC collagen production and medial fibrosis. We previously demonstrated that forced miR-29b downregulation (via systemic anti-miR administration) is a profibrotic intervention reducing AAA growth.[16] This reduction, in light of the present study, may be partially attributable to accelerated miR-29b–dependent stiffening of the AAA-adjacent aorta.

Local aortic PPE infusion is a widely used preclinical AAA model that exhibits many features seen in human AAA, including early disturbance of elastin integrity. However, because of the artificial, invasive nature of the model, including enzymatic injury of the vessel, segmental stiffness might be model specific and not a feature of human AAA. We therefore studied whether the human abdominal aorta exhibits segmental stiffness that, according to our hypothesis, would be a contributing factor for AAA formation. Performing ultrasound-based strain analyses in 3 distinct locations along the abdominal aorta (suprarenal, midinfrarenal, bifurcation), we detected age-dependent reduction of strain (increased stiffness), corresponding to previous observations.[42] As a novel finding, we detected relatively more pronounced stiffening of the aortic bifurcation segment with age (Figure 8C), translating into increasing SAS of the aortic bifurcation over time (Figure 8D). This distal part of the aorta has relatively low elastin content in comparison with the more proximal segments,[43] a feature that might become functionally relevant with age-dependent loss of elastin.[15] These data confirm and refine previous observations of enhanced age-dependent stiffening of the abdominal aorta[10] and might explain, in part, the significant influence of age on AAA risk.

Of note, the segmental stiffness we observed in the human abdominal aorta (SAS ≈2) was significantly smaller than the peak segmental stiffness in the PPE-treated aorta (SAS ≈5). The study patients presumably exhibited physiological stiffness segmentation that will most likely not result in AAA formation. However, segmental stiffening may have more dramatic effects in individuals with genetic predilection for aneurysm formation.

In conclusion, the present study introduces the novel concept of SAS as a pathogenetic factor contributing to AAA. We propose that degenerative stiffening of the aneurysm-prone aortic wall leads to axial stress, generated by cyclic tethering of adjacent, more compliant wall segments. Axial stress then induces and augments processes necessary for AAA growth such as inflammation and vascular wall remodeling (Figure VII online-only Data Supplement). Clarification of these biomechanical signaling pathways may lead to additional therapeutic targets.

From a diagnostic point of view, AAA characterization has almost exclusively focused on the dilated segment. In light of the present findings, additional mechanical characterization of the AAA-adjacent aortic segments might provide important insights into the stress status of the aneurysm. This might be of particular relevance in early (even preaneurysmal) stages of disease, when mechanical stress is not yet predominantly driven by large geometric alterations. For instance, ultrasound-derived SAS assessment might help to predict the susceptibility for AAA formation and future AAA growth. Therefore, SAS could practically be useful to individualize risk prediction for patient populations at generally increased risk for AAA (eg, smokers, family history) or to better determine monitoring intervals for patients with small AAA. Having a more sensitive and specific indicator for clinical progression may improve decision making in AAA disease, and help direct resources to those in need in an increasingly resource-constrained environment.

From a therapeutic perspective, this study suggests that mechanically stiffening the AAA-adjacent aorta might provide a stress shield to limit AAA remodeling and expansion. This is supported in principle by recent data suggesting reduced growth rate of suprarenal AAAs in patients having undergone endovascular repair of a concomitant infrarenal AAA (in comparison with control patients without infrarenal repair).[44] Of note, protective interventional stiffening of an AAA-adjacent segment may create a distal stiffness gradient along the arterial tree that potentially triggers distal aneurysm formation. However, we did not observe any evidence of this during the 28-day time course of our model. This may indicate that, in addition to stiffness gradients, other predisposing cofactors (eg, a structurally impaired vessel matrix) may be required to trigger AAA formation de novo. Further, we did not detect

increased blood pressure levels after interventional stiffening of the abdominal aorta that could potentially point toward negative hemodynamic side effects (Table I online-only Data Supplement). Therefore, interventional stiffening of the aortic segment next to a small aneurysm could be further tested as a novel approach to limit further AAA progression, and forestall surgical repair.

Acknowledgments

We thank Tiffany K. Koyano, Yanli Wang, Michelle Ramseier, and Brian Deng for expert technical assistance. We further thank Hui Wang, Ying Lu, Balasubramanian Narasimhan, and Bradley Efron for expert statistical consulting.

Sources of Funding

This work was supported by research grants from the NIH (1R01HL105299 to Dr Tsao), the Deutsche Forschungsgemeinschaft (RA 2179/1-1 to Dr Raaz), the Stanford Graduate Fellowship (William R. and Sara Hart Kimball Fellowship to A. M. Zöllner), the University of Erlangen-Nuremberg School of Medicine (to I. N. Schellinger), and the Stanford Cardiovascular Institute (to Dr Spin).

Disclosures

None.

References

1. Nordon IM, Hinchliffe RJ, Loftus IM, Thompson MM. Pathophysiology and epidemiology of abdominal aortic aneurysms. *Nat Rev Cardiol*. 2011;8:92–102. doi: 10.1038/nrcardio.2010.180.
2. Shah PK. Inflammation, metalloproteinases, and increased proteolysis: an emerging pathophysiological paradigm in aortic aneurysm. *Circulation*. 1997;96:2115–2117.
3. Ailawadi G, Eliason JL, Upchurch GR Jr. Current concepts in the pathogenesis of abdominal aortic aneurysm. *J Vasc Surg*. 2003;38:584–588.
4. Raaz U, Toh R, Maegdefessel L, Adam M, Nakagami F, Emrich FC, Spin JM, Tsao PS. Hemodynamic regulation of reactive oxygen species: implications for vascular diseases. *Antioxid Redox Signal*. 2014;20:914–928. doi: 10.1089/ars.2013.5507.
5. Hoefer IE, den Adel B, Daemen MJ. Biomechanical factors as triggers of vascular growth. *Cardiovasc Res*. 2013;99:276–283. doi: 10.1093/cvr/cvt089.
6. Vorp DA. Biomechanics of abdominal aortic aneurysm. *J Biomech*. 2007;40:1887–1902. doi: 10.1016/j.jbiomech.2006.09.003.
7. Humphrey JD, Holzapfel GA. Mechanics, mechanobiology, and modeling of human abdominal aorta and aneurysms. *J Biomech*. 2012;45:805–814. doi: 10.1016/j.jbiomech.2011.11.021.
8. MacSweeney ST, Young G, Greenhalgh RM, Powell JT. Mechanical properties of the aneurysmal aorta. *Br J Surg*. 1992;79:1281–1284.
9. Vande Geest JP, Sacks MS, Vorp DA. The effects of aneurysm on the biaxial mechanical behavior of human abdominal aorta. *J Biomech*. 2006;39:1324–1334. doi: 10.1016/j.jbiomech.2005.03.003.
10. Hickson SS, Butlin M, Graves M, Taviani V, Avolio AP, McEniery CM, Wilkinson IB. The relationship of age with regional aortic stiffness and diameter. *JACC Cardiovasc Imaging*. 2010;3:1247–1255. doi: 10.1016/j.jcmg.2010.09.016.
11. Azuma J, Asagami T, Dalman R, Tsao P. Creation of murine experimental abdominal aortic aneurysms with elastase. *J Vis Exp*. 2009;29:1280.
12. Hong G, Lee JC, Robinson JT, Raaz U, Xie L, Huang NF, Cooke JP, Dai H. Multifunctional *in vivo* vascular imaging using near-infrared II fluorescence. *Nat Med*. 2012;18:1841–1846. doi: 10.1038/nm.2995.
13. Sho E, Sho M, Nanjo H, Kawamura K, Masuda H, Dalman RL. Comparison of cell-type-specific vs transmural aortic gene expression in experimental aneurysms. *J Vasc Surg*. 2005;41:844–852. doi: 10.1016/j.jvs.2005.02.027.
14. He CM, Roach MR. The composition and mechanical properties of abdominal aortic aneurysms. *J Vasc Surg*. 1994;20:6–13.
15. Fritze O, Romero B, Schleicher M, Jacob MP, Oh DY, Starcher B, Schenke-Layland K, Bujan J, Stock UA. Age-related changes in the elastic tissue of the human aorta. *J Vasc Res*. 2012;49:77–86. doi: 10.1159/000331278.
16. Maegdefessel L, Azuma J, Toh R, Merk DR, Deng A, Chin JT, Raaz U, Schoelmerich AM, Raiesdana A, Leeper NJ, McConnell MV, Dalman RL, Spin JM, Tsao PS. Inhibition of microRNA-29b reduces murine abdominal aortic aneurysm development. *J Clin Invest*. 2012;122:497–506. doi: 10.1172/JCI61598.
17. Goergen CJ, Azuma J, Barr KN, Magdefessel L, Kallop DY, Gogineni A, Grewall A, Weimer RM, Connolly AJ, Dalman RL, Taylor CA, Tsao PS, Greve JM. Influences of aortic motion and curvature on vessel expansion in murine experimental aneurysms. *Arterioscler Thromb Vasc Biol*. 2011;31:270–279. doi: 10.1161/ATVBAHA.110.216481.
18. Pyo R, Lee JK, Shipley JM, Curci JA, Mao D, Ziporin SJ, Ennis TL, Shapiro SD, Senior RM, Thompson RW. Targeted gene disruption of matrix metalloproteinase-9 (gelatinase B) suppresses development of experimental abdominal aortic aneurysms. *J Clin Invest*. 2000;105:1641–1649. doi: 10.1172/JCI8931.
19. Qiu J, Zheng Y, Hu J, Liao D, Gregersen H, Deng X, Fan Y, Wang G. Biomechanical regulation of vascular smooth muscle cell functions: from *in vitro* to *in vivo* understanding. *J R Soc Interface*. 2014;11:20130852. doi: 10.1098/rsif.2013.0852.
20. Zampetaki A, Zhang Z, Hu Y, Xu Q. Biomechanical stress induces IL-6 expression in smooth muscle cells via Ras/Rac1-p38 MAPK-NF-kappaB signaling pathways. *Am J Physiol Heart Circ Physiol*. 2005;288:H2946–H2954. doi: 10.1152/ajpheart.00919.2004.
21. Riou S, Mees B, Esposito B, Merval R, Vilar J, Stengel D, Ninio E, van Haperen R, de Crom R, Tedgui A, Lehoux S. High pressure promotes monocyte adhesion to the vascular wall. *Circ Res*. 2007;100:1226–1233. doi: 10.1161/01.RES.0000265231.59354.2c.
22. Miller FJ. Oxidative stress in human abdominal aortic aneurysms: a potential mediator of aneurysmal remodeling. *Arterioscler Thromb Vasc Biol*. 2002;22:560–565.
23. Matsushita H, Lee KH, Tsao PS. Cyclic strain induces reactive oxygen species production via an endothelial NAD(P)H oxidase. *J Cell Biochem Suppl*. 2001;(suppl 36):99–106.
24. Grote K, Flach I, Luchtefeld M, Akin E, Holland SM, Drexler H, Schieffer B. Mechanical stretch enhances mRNA expression and proenzyme release of matrix metalloproteinase-2 (MMP-2) via NAD(P)H oxidase-derived reactive oxygen species. *Circ Res*. 2003;92:e80–e86. doi: 10.1161/01.RES.0000077044.60138.7C.
25. Li PF, Dietz R, von Harsdorf R. Reactive oxygen species induce apoptosis of vascular smooth muscle cell. *FEBS Lett*. 1997;404:249–252.
26. Gavrila D, Li WG, McCormick ML, Thomas M, Daugherty A, Cassis LA, Miller FJ Jr, Oberley LW, Dellsperger KC, Weintraub NL. Vitamin E inhibits abdominal aortic aneurysm formation in angiotensin II-infused apolipoprotein E-deficient mice. *Arterioscler Thromb Vasc Biol*. 2005;25:1671–1677. doi: 10.1161/01.ATV.0000172631.50972.0f.
27. Nakahashi TK, Hoshina K, Tsao PS, Sho E, Sho M, Karwowski JK, Yeh C, Yang RB, Topper JN, Dalman RL. Flow loading induces macrophage antioxidative gene expression in experimental aneurysms. *Arterioscler Thromb Vasc Biol*. 2002;22:2017–2022.
28. Xiong W, Mactaggart J, Knispel R, Worth J, Zhu Z, Li Y, Sun Y, Baxter BT, Johanning J. Inhibition of reactive oxygen species attenuates aneurysm formation in a murine model. *Atherosclerosis*. 2009;202:128–134. doi: 10.1016/j.atherosclerosis.2008.03.029.
29. Yang JH, Sakamoto H, Xu EC, Lee RT. Biomechanical regulation of human monocyte/macrophage molecular function. *Am J Pathol*. 2000;156:1797–1804. doi: 10.1016/S0002-9440(10)65051-1.
30. Johnston WF, Salmon M, Su G, Lu G, Stone ML, Zhao Y, Owens GK, Upchurch GR Jr, Ailawadi G. Genetic and pharmacologic disruption of interleukin-1β signaling inhibits experimental aortic aneurysm formation. *Arterioscler Thromb Vasc Biol*. 2013;33:294–304. doi: 10.1161/ATVBAHA.112.300432.
31. Tieu BC, Lee C, Sun H, Lejeune W, Recinos A 3rd, Ju X, Spratt H, Guo DC, Milewicz D, Tilton RG, Brasier AR. An adventitial IL-6/MCP1 amplification loop accelerates macrophage-mediated vascular inflammation leading to aortic dissection in mice. *J Clin Invest*. 2009;119:3637–3651. doi: 10.1172/JCI38308.
32. Moehle CW, Bhamidipati CM, Alexander MR, Mehta GS, Irvine JN, Salmon M, Upchurch GR Jr, Kron IL, Owens GK, Ailawadi G. Bone marrow-derived MCP1 required for experimental aortic aneurysm formation and smooth muscle phenotypic modulation. *J Thorac Cardiovasc Surg*. 2011;142:1567–1574. doi: 10.1016/j.jtcvs.2011.07.053.
33. Freestone T, Turner RJ, Coady A, Higman DJ, Greenhalgh RM, Powell JT. Inflammation and matrix metalloproteinases in the enlarging abdominal aortic aneurysm. *Arterioscler Thromb Vasc Biol*. 1995;15:1145–1151.
34. Thompson RW, Holmes DR, Mertens RA, Liao S, Botney MD, Mecham RP, Welgus HG, Parks WC. Production and localization of 92-kilodalton

gelatinase in abdominal aortic aneurysms. An elastolytic metalloproteinase expressed by aneurysm-infiltrating macrophages. *J Clin Invest*. 1995;96:318–326. doi: 10.1172/JCI118037.
35. Davis V, Persidskaia R, Baca-Regen L, Itoh Y, Nagase H, Persidsky Y, Ghorpade A, Baxter BT. Matrix metalloproteinase-2 production and its binding to the matrix are increased in abdominal aortic aneurysms. *Arterioscler Thromb Vasc Biol*. 1998;18:1625–1633.
36. Longo GM, Xiong W, Greiner TC, Zhao Y, Fiotti N, Baxter BT. Matrix metalloproteinases 2 and 9 work in concert to produce aortic aneurysms. *J Clin Invest*. 2002;110:625–632. doi: 10.1172/JCI15334.
37. Castier Y, Brandes RP, Leseche G, Tedgui A, Lehoux S. p47phox-dependent NADPH oxidase regulates flow-induced vascular remodeling. *Circ Res*. 2005;97:533–540. doi: 10.1161/01.RES.0000181759.63239.21.
38. Jackson ZS. Wall tissue remodeling regulates longitudinal tension in arteries. *Circ Res*. 2002;90:918–925.
39. Maegdefessel L, Azuma J, Toh R, Deng A, Merk DR, Raiesdana A, Leeper NJ, Raaz U, Schoelmerich AM, McConnell MV, Dalman RL, Spin JM, Tsao PS. MicroRNA-21 blocks abdominal aortic aneurysm development and nicotine-augmented expansion. *Sci Transl Med*. 2012;4:122ra22. doi: 10.1126/scitranslmed.3003441.
40. Thompson RW, Liao S, Curci JA. Vascular smooth muscle cell apoptosis in abdominal aortic aneurysms. *Coron Artery Dis*. 1997;8:623–631.
41. Hoit BD, Kiatchoosakun S, Restivo J, Kirkpatrick D, Olszens K, Shao H, Pao YH, Nadeau JH. Naturally occurring variation in cardiovascular traits among inbred mouse strains. *Genomics*. 2002;79:679–685. doi: 10.1006/geno.2002.6754.
42. O'Rourke MF, Hashimoto J. Mechanical factors in arterial aging: a clinical perspective. *J Am Coll Cardiol*. 2007;50:1–13. doi: 10.1016/j.jacc.2006.12.050.
43. Halloran BG, Davis VA, McManus BM, Lynch TG, Baxter BT. Localization of aortic disease is associated with intrinsic differences in aortic structure. *J Surg Res*. 1995;59:17–22. doi: 10.1006/jsre.1995.1126.
44. Herdrich BJ, Murphy EH, Wang GJ, Jackson BM, Fairman RM, Woo EY. The fate of untreated concomitant suprarenal aortic aneurysms after endovascular aneurysm repair of infrarenal aortic aneurysms. *J Vasc Surg*. 2013;58:1201–1206. doi: 10.1016/j.jvs.2013.05.009.

CLINICAL PERSPECTIVE

Abdominal aortic aneurysm (AAA) is a common and potentially lethal disease of the aging aorta. Many AAAs remain asymptomatic until fatal rupture. Current treatment is limited to larger aneurysms (typically AAA diameter >5.5 cm) and consists of open surgery or stent-based intervention. Therefore, there is a need for improved risk stratification and disease monitoring, as well as for early treatment options. The present study mechanistically links segmental aortic stiffening (SAS), a feature of aortic aging, to subsequent AAA development. Moreover, it provides preclinical evidence that interventional stiffening of the AAA-adjacent aorta may provide a mechanical stress shield to limit AAA expansion. Those findings give rise to potential diagnostic and therapeutic benefits. From a diagnostic point of view, ultrasound-based assessment of SAS, for instance, might help to predict the susceptibility for AAA formation and future AAA enlargement. Therefore, the parameter SAS could be of practical use for personalized AAA risk prediction in patient populations at a generally increased risk for the disease (eg, smokers, patients with family history for AAA). Further, SAS could be helpful to better determine monitoring intervals for patients with already established small AAA. From a therapeutic perspective, interventional stiffening of the aortic segment next to a developing aneurysm could be further tested as a novel approach to limit AAA progression and to forestall surgical repair.

SUPPLEMENTAL MATERIAL

Segmental aortic stiffening contributes to experimental abdominal aortic aneurysm development

Uwe Raaz,MD[1,2,3]; Alexander M. Zöllner,MS[4,2]; Isabel N. Schellinger[1,3]; Ryuji Toh,MD,PhD[1]; Futoshi Nakagami,MD,PhD[1,2]; Moritz Brandt,MD[2]; Fabian C. Emrich,MD[5,2]; Yosuke Kayama,MD,PhD[1,2,3]; Suzanne Eken,MD[6]; Matti Adam,MD[1,2,3]; Lars Maegdefessel,MD,PhD[6]; Thomas Hertel,MD[7]; Alicia Deng[1,3]; Ann Jagger,PhD[1,3]; Michael Buerke,MD[8]; Ronald L. Dalman,MD[9,2]; Joshua M. Spin,MD,PhD[1,2,3]; Ellen Kuhl,PhD[4,10,5]; Philip S. Tsao,PhD[1,2,3]

[1]Division of Cardiovascular Medicine, Stanford University School of Medicine, Stanford, CA; [2]Cardiovascular Institute, Stanford University School of Medicine, Stanford, CA; [3]VA Palo Alto Health Care System, Palo Alto, CA; [4]Department of Mechanical Engineering, Stanford University School of Medicine, Stanford, CA; [5]Department of Cardiothoracic Surgery, Stanford University School of Medicine, Stanford, CA; [6]Department of Medicine, Karolinska Institute, Stockholm, Sweden; [7]Center for Vascular Medicine, Zwickau, Germany; [8]Division of Cardiovascular Medicine and Intensive Care Medicine, Saint Mary's Hospital, Siegen, Germany; [9]Division of Vascular Surgery, Stanford University School of Medicine, Stanford, CA; [10]Department of Bioengineering, Stanford, CA

Supplemental Methods

Mouse ultrasound studies

Mice were anesthetized using 1.5% isoflurane (Vet One, Meridian, ID, USA) and imaged in a supine position on a heated platform. Imaging was performed using a real-time microvisualization transducer (MS550D) with a frequency of 40 MHz connected to a Vevo 2100 ultrasound system (Visualsonics, Toronto, Canada). Initially the abdominal aorta was visualized in B-mode in a longitudinal orientation. M-mode images tracking the anterior and posterior aortic wall motion were then recorded in a perpendicular orientation at specific locations along the infrarenal aorta. Multiple cardiac cycles (at least 6) were recorded and the acquired images were stored digitally on a built-in hard drive for offline analysis. All measurements were collected by one observer to limit bias, while a second independent observer, blinded to the treatment group, analyzed the recordings.

Image analysis was performed using the accompanying Vevo770 software (Visualsonics, Toronto, Canada). Systolic diameter (D_s) and diastolic diameter (D_d) were quantified in the PPE-treated segment as well as in the adjacent untreated aortic segments. Circumferential cyclic strain $\varepsilon$was calculated as $\varepsilon = (D_s-D_d)/D_d$ x 100%. Segmental aortic stiffness (SAS) was defined as a relative index to quantify the stiffness of the PPE-treated segment in relation to the adjacent aorta. Therefore it was calculated as SAS = $\varepsilon_{\text{adjacent aorta}} / \varepsilon_{\text{PPE segment}}$. The strain values for the adjacent aorta ($\varepsilon_{\text{adjacent aorta}}$) represent an average strain calculated from the adjacent segments proximal and distal from the PPE-treated segment. For shear stress calculations blood flow was assessed as previously described[1]. In short, peak flow velocity (V) was quantified by pw-Doppler measurements in the PPE-treated aortic segments. Flow was then calculated as $Q = V\pi(D_s/2)^2$. Wall shear stress was

calculated using the Poiseuille formula, $\tau = 4\mu Q/\pi(Ds/2)^3$. The viscosity of blood (μ) was taken to be 0.035 poise.

Human ultrasound studies

19 male volunteers of different ages (youngest age: 36, oldest age: 71 mean age: 51.9 years) were included in the study. Exclusion criteria were cardiovascular diseases (in particular AAA), diabetes and history of smoking. Volunteers were imaged in supine position using an ACUSON X300 PE ultrasound system (Siemens, Germany) with a curved abdominal transducer (CH5-2) using a frequency of 1.8 MHz (Tissue Harmonic Imaging). The abdominal aorta was visualized in B-mode in a longitudinal orientation. M-mode images tracking the anterior and posterior aortic wall motion were then recorded in a perpendicular orientation at predefined locations (suprarenal, mid-infrarenal and proximal of the aortic bifurcation). Multiple cardiac cycles (at least 4) were recorded and the acquired images were stored digitally. All measurements were collected by one observer to limit bias, while a second independent observer, blinded to the patient's characteristics, analyzed the recordings.

Image analysis was performed using ImageJ software (National Institutes of Health, Bethesda, MD, USA). Systolic diameter (D_s) and diastolic diameter (D_d) were quantified in the suprarenal, mid-infrarenal and bifurcational segment of the abdominal aorta. Circumferential cyclic strain ε was calculated as $\varepsilon = (D_s-D_d)/D_d$ x 100%. Segmental aortic stiffness (SAS) along the infrarenal abdominal aorta was calculated as SAS = $\varepsilon_{\text{mid-infrarenal aorta}} / \varepsilon_{\text{bifurcational segment}}$.

Finite element analysis (FEA)

Finite element analyses of the mouse aorta were performed using the commercial finite element software package ABAQUS. The artery was modeled as a 2.0 mm long axisymmetric tube with outer diameter D_a=0.9 mm and arterial wall thickness t=0.075 mm. Between 10600 and 17100 axisymmetric 4-node bilinear hybrid elements (CAX4) were used for the configurations with and without BioGlue, respectively. Dirichlet boundary conditions were imposed in the transverse mid plane to enforce symmetry, while von Neumann boundary conditions were applied on the interior wall to model the arterial pressure. The intima, media, and adventitia were summarized in a single homogeneous layer modeled using an isotropic Neo-Hookean strain energy function with a shear modulus of 300 kPa. Stiffness of the stiff segment (l=1.0 mm) was modified as indicated. Material properties of BioGlue were adapted from reference [2].

Preparation of aortic tissue for RNA extraction

Mice were sacrificed with an inhalation overdose of isoflurane (Vet One, Meridian, ID, USA). Immediately following sacrifice the abdominal aorta was transected and flushed via the left ventricle with ice cold phosphate buffered saline (PBS; pH 7.4). The aorta was then dissected from fat and connective tissue from the left renal artery to the bifurcation under a microscope (Leica, Wetzlar, Germany). Specimens were snap-frozen individually in liquid nitrogen and stored at -80°C before further processing.

RNA quantification

Total RNA was isolated using a TRIzol-based (Invitrogen) RNA isolation protocol. RNA was quantified by Nanodrop (Agilent Technologies), and RNA and miRNA

quality were verified using an Agilent 2100 Bioanalyzer (Agilent Technologies). Samples required 260/280 ratios >1.8, and sample RNA integrity numbers >9 for inclusion. For mRNA studies, the iScript cDNA synthesis kit (Bio-Rad) was used to synthesize first-strand cDNA according to the manufacturer's protocol. TaqMan qRT-PCR assay was performed using mouse specific primers (Applied Biosystems) for: *Col1a1*, *Col3a1*, *Mmp2*, *Mmp9*, *IL6*, *Il1b*, *Ccl2, and Emr1*. All probes were normalized to 18S as internal control. For microRNA studies RNA was reverse transcribed using the TaqMan microRNA Reverse Transcription kit (Applied Biosystems) according to the manufacturer's instructions. MicroRNA and TaqMan assay kits (Applied Biosystems) for hsa-miR-29b and sno202 (endogenous control for normalization in mice) were used. Amplification took place on a QuantStudio12K Flex (Applied Biosystems). All fold changes were calculated by the method of ΔΔCt. All experiments included $\geq$ 5 samples per group.

Tissue preparation for histological analysis

Mice were euthanized and perfused at a constant pressure of 100 mmHg via the left ventricle with saline followed by warm (37°C) agarose gel (Amresco) diluted in saline (3% w/v). After the agarose solidified, the abdominal aorta was dissected free from the surrounding connective tissue and fixed in 4% formalin. The isolated abdominal aorta was then dehydrated through a graded sucrose series and subsequently embedded in OCT blocks. For in situ DHE oxidation the aortas were dissected and OCT embedded without any prior fixation.

Laser capture microdissection

Freshly cut aortic cross sections (7μm) were fixed in ice-cold 75% ethanol for 30 s, washed in ice-cold PBS, stained with FITC-labeled F4/80 antibody diluted in Sea

Block buffer (both Abcam) for 1 min, rinsed in ice-cold PBS, incubated in ice-cold 75% ethanol for 30 s and ice-cold 100% ethanol for 30 s, and desiccated by two 1-min xylene incubations. Laser ablation was carried out after stage calibration, laser focus, and optical focus calibration as per manufacturer's instructions, in a Zeiss Observer Z1 inverted microscope outfitted with PALM Microbeam (Zeiss). Ablated cells were catapulted by laser pressure catapulting (LPC) bursts into Zeiss AdhesiveCap 500 ml tubes. Cell capture was verified by direct observation of the adhesive collection cap. Directly following microdissection cells were lysed, cellular RNA was reverse-transcribed and cDNA was pre-amplified using the Single Cell-to-CT Kit (Ambion). Subsequently qRT-PCR was performed on a QuantStudio12K Flex (Applied Biosystems). All fold changes were calculated by the method of ΔΔCt with Gapdh serving as internal control. Individual samples contained cellular material dissected from 3 individual aortic sections. All experiments included 4 samples per group.

Picrosirius Red staining

Aortic cross sections (7µm) were stained using the Picrosirius Red stain kit (American MasterTech, USA) according to manufacturer's instructions. In brief, nuclei were stained using Weigert's hematoxylin. Samples were then washed in running tap water for 10 minutes, stained in Picrosirius Red for 1h, washed in 0.5% acetified water, dehydrated in 100% ethanol, cleared in xylene, and mounted using a resinous medium.

Elastin Verhoeff's Van Gieson Staining

Aortic cross sections (7μm) were stained stained with the Modified Elastin Verhoeff Van Gieson (VVG) Elastic Stain Kit (Sigma Aldrich, St. Louis, MO, USA) according to manufacturer's protocol.

Immunofluorescence

Aortic cross sections (7μm) were fixed for 15 minutes in 4% PFA and PBS. Primary antibodies against F4/80 (rat), Il-6 (rabbit), Il-1β (rabbit), and activated Caspase 3 (rabbit) (all Abcam) were applied overnight. Incubation with secondary antibodies (Alexa Fluor 594 goat anti-rat, Alexa Fluor 594 goat anti rabbit, and Alexa Fluor 488 donkey anti rabbit; Molecular Probes) was performed for 1 hour. Counterstaining was performed with Hoechst reagent (bisBenzide H 33258) (Sigma-Aldrich, St. Louis, MO, USA). Negative controls were performed with the omission of the primary antibody. Imaging was performed using a Leica DM4000B (Buffalo Grove, IL, USA).

In situ DHE staining

The amount of intracellular ROS production was determined using dihydroethidium (DHE) (Molecular Probes - red fluorescence). Frozen aortic cross sections (7 μm) were mounted on glass slides, rinsed in PBS, and incubated in 10 μM DHE (37°C, 30 minutes). Intensity was measured by fluorescence microscopy (Leica DM4000B; Buffalo Grove, IL, USA) using a Texas red filter (488-nm excitation, 610-nm emission). Autofluorescence from elastic lamellae was subtracted, and fluorescence was quantified using ImageJ (National Institutes of Health, Bethesda, MD, USA)

In situ hybridization (ISH)

ISH for miR-29b was performed by using the miRCURY LNA microRNA ISH Optimization Kit (Exiqon) and 5'-DIG‐and 3'-DIG‐ labeled probes for mmu-miR-29b according to the manufacturer's protocol.

Ex vivo *aortic mechanical stimulation*

The abdominal aorta was explanted from 10-week-old male C57BL/6J, placed on specially designed stainless steel cannulas and secured with silk surgical suture (10-0). Aortas were mounted in the heated vessel chamber of a pressure arteriograph system (Model 110P, Danish Myotechnology, Copenhagen, Denmark) and stretched to *in vivo* length. Physiological saline solution (PSS) at 37°C, aerated with 5% CO2/ 95% O2 was used to fill the vessel chamber and for aortic perfusion. The aorta was then subjected to an automated pressure protocol, cyclically alternating between 80 mmHg and 120 mmHg with a frequency of 4/min for one hour. To stiffen/restrain either the complete aorta or just the central segment (to simulate segmental stiffening), a silicone cuff (SILASTIC Laboratory Tubing, inner diameter: 0.51mm; Dow Corning) was tied around the aorta (Supplemental Figure S6). After conclusion of the experiment the aorta was removed from the cannulas and processed for RNA isolation.

Blood pressure measurements

Blood pressure measurements were performed using non-invasive VPR (Volume-Pressure Recording) tail cuff sensor technology (CODA System; Kent Scientific). All mice were acclimated to the restrainer for 10–20 min per day for at least 3 consecutive days before starting the study. Following this acclimation period, mice remained calm and still in the restrainer on the day of testing. To facilitate the

acclimation process, the mice were handled gently and not forced to enter the restrainer, and the ambient temperature was maintained at warm room temperature (25–30°C).

References

1. Hong G, Lee J, Robinson J, Raaz U, Xie L, Huang N, Cooke J and Dai H.Multifunctional in vivo vascular imaging using near-infrared II fluorescence.*Nat Med*.2012;18:1841-6.

2. Azadani A, Matthews P, Ge L, Shen Y, Jhun C, Guy T and Tseng E.Mechanical properties of surgical glues used in aortic root replacement.*Ann Thorac Surg*.2009;87:1154-60.

Supplemental tables

	Glue (n=5)	Sham (n=5)	p value
SBP	128 ± 2	127 ± 3	0.627
DBP	100 ± 3	105 ± 3	0.826
MAP	110 ± 3	113 ± 3	0.888
PP	27 ± 2	25 ± 2	0.948

Table S1: Blood pressure measurements in glue- or sham-treated mice 7 days after PPE-induction. SBP indicates systolic blood pressure, DBP diastolic blood pressure, MAP mean arterial pressure, PP pulse pressure (=SBP-DBP).

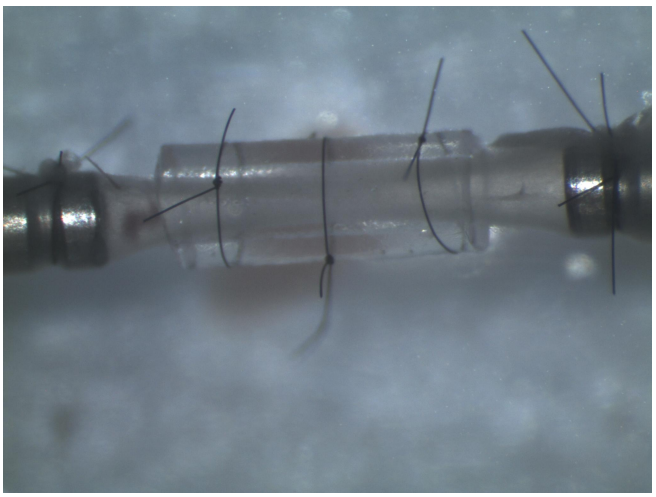

Figure S1: Setup for differential mechanical stimulation of the murine aorta *ex vivo*. The abdominal aorta is mounted between to two steel cannulas. A silicone cuff has been tied around the central aortic segment.

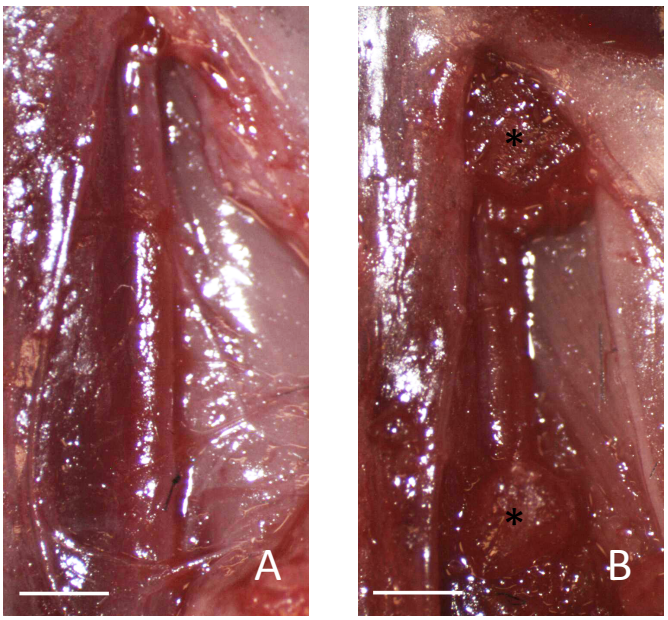

Figure S2: Application of surgical glue. Depicted is the abdominal aorta before (A) and after (B) glue (*) application to the segments adjacent to the PPE-treated segment. Scale bar represents 1mm.

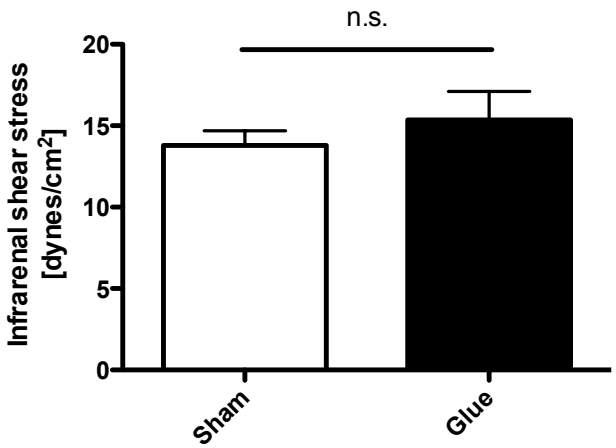

Figure S3: Shear stress occurring in the PPE-treated segment. Ultrasound measurements for shear stress calculation were taken at day 7 after PPE-induction.

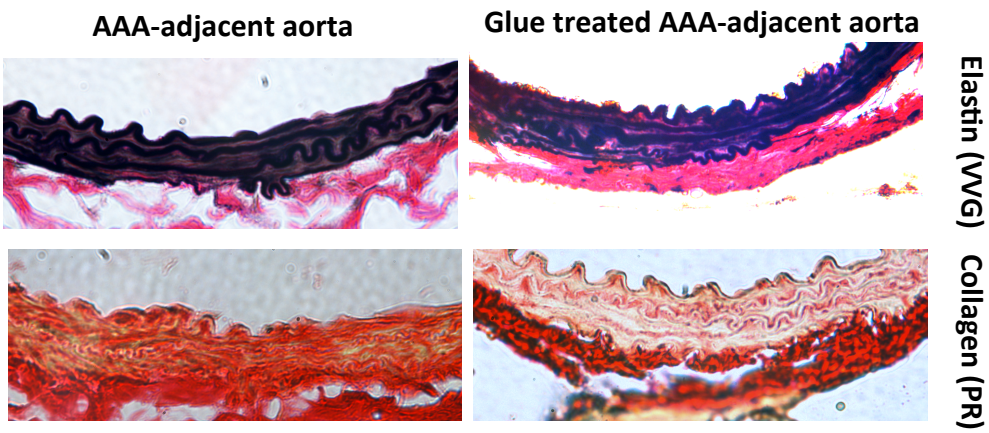

Figure S4: Elastin architecture (Verhoef Van Gieson staining; upper panels) and collagen depostion (Picrosirius Red staining; lower panels) of the AAA-adjacent aorta (day 14) with (right panels) and without glue treatment (left panels). While the elastin architecture of the aortic wall is unaffected by surrounding glue-treatment collagen deposition is reduced (possibly reflecting an effect of mechanical offloading of the glue-stiffened aorta).

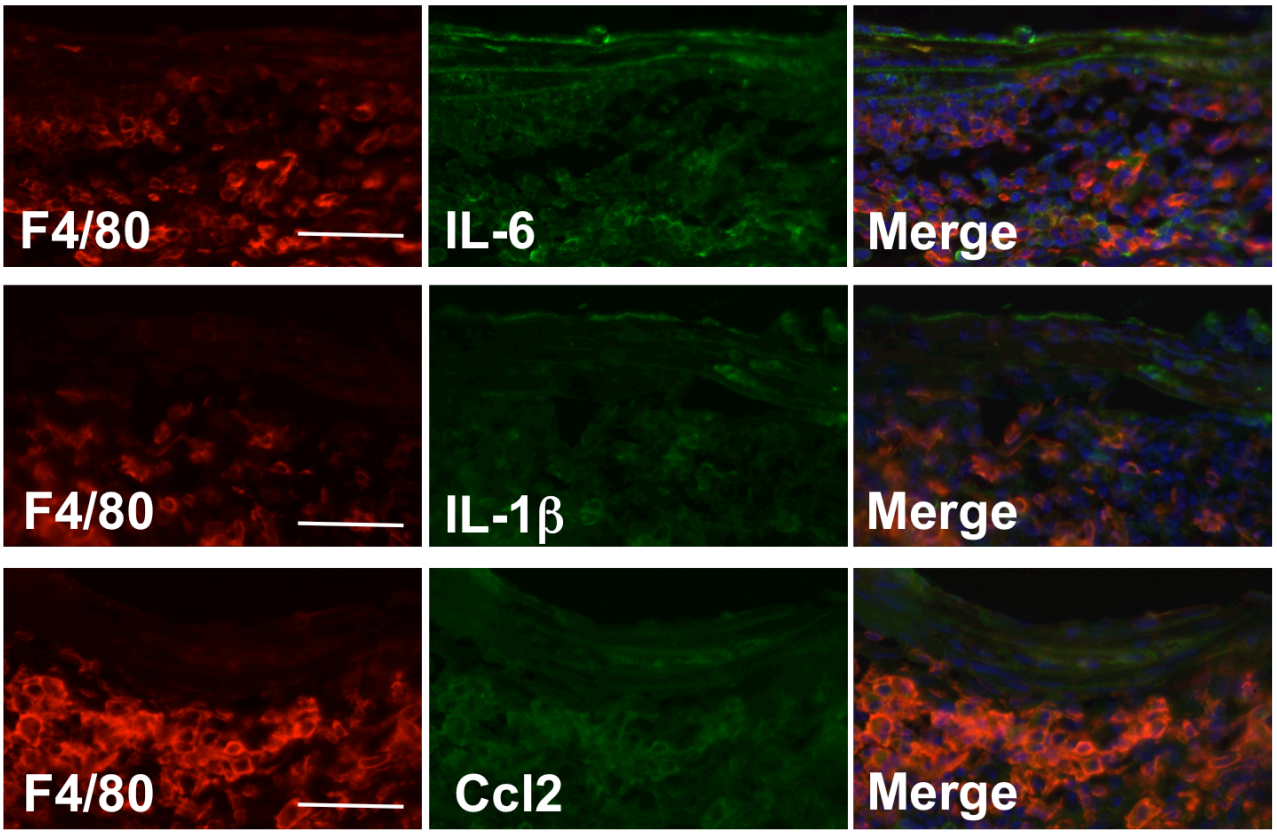

Figure S5: Immunofluorescence macrophage co-staining for inflammatory cytokines Il-6, IL-1β and Ccl2 on day 7 after PPE-treatment. Macrophages (F4/80) are stained red (left panels), while Il-6, IL-1β and Ccl2 are shown in green (middle panels). Merged images (right panels) demonstrate macrophages co-localize with cytokines (orange). Nuclei are stained blue (Hoechst) in merged pictures.

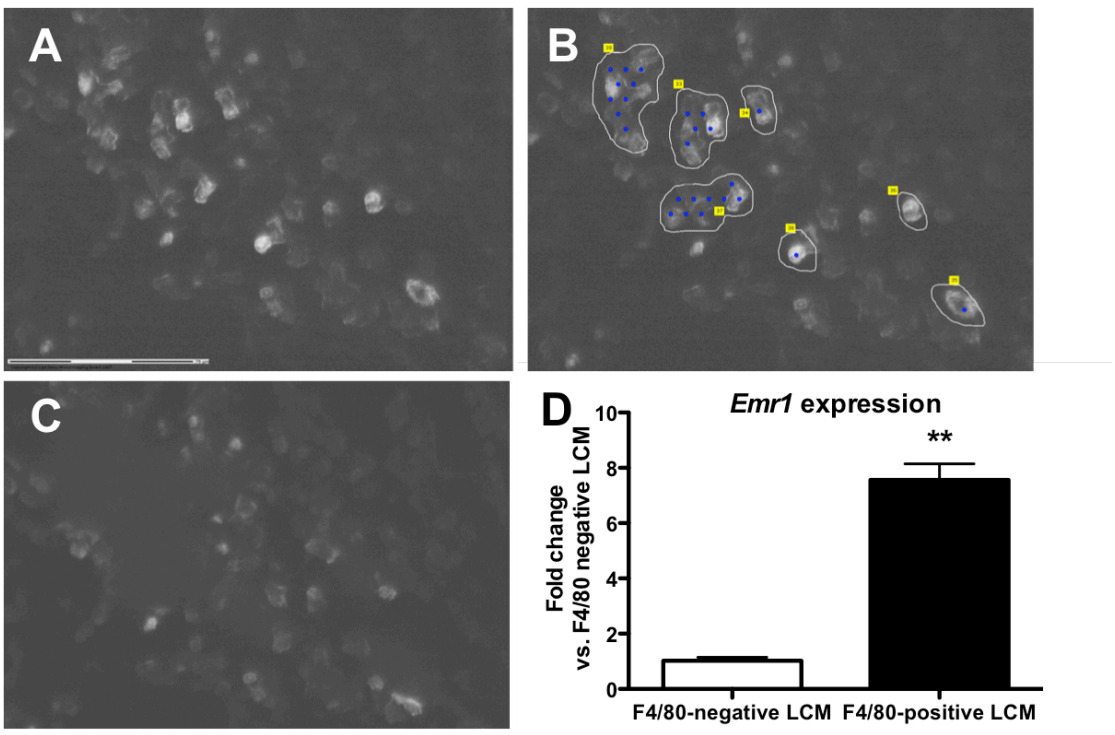

Figure S6: Macrophage isolation via laser capture microdissection (LCM). Macrophages (with F4/80-fluorescent label; A) were selectively targeted (B) and isolated (C) via LCM. Macrophage transcript enrichment was confirmed via enhanced *Emr1* expression compared to LCM-isolated F4/80-negative cells. ** indicates $p < 0.001$

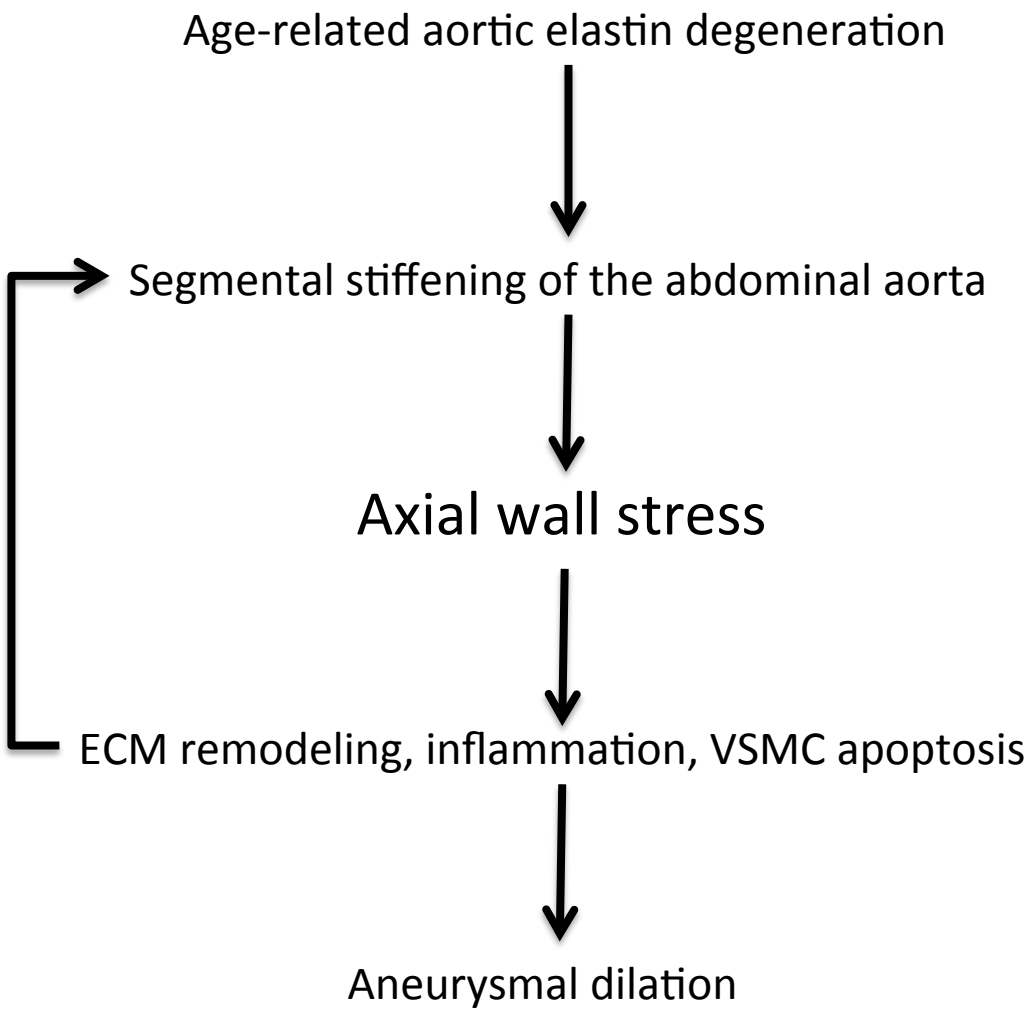

Figure S7. Proposed mechanism of early AAA formation driven by age-related segmental aortic stiffening. Degenerative segmental stiffening of the abdominal aorta induces axial stress in the stiff segment, thereby promoting active inflammatory wall remodeling resulting in AAA formation.

Segmental Aortic Stiffening Contributes to Experimental Abdominal Aortic Aneurysm Development

Uwe Raaz, Alexander M. Zöllner, Isabel N. Schellinger, Ryuji Toh, Futoshi Nakagami, Moritz Brandt, Fabian C. Emrich, Yosuke Kayama, Suzanne Eken, Matti Adam, Lars Maegdefessel, Thomas Hertel, Alicia Deng, Ann Jagger, Michael Buerke, Ronald L. Dalman, Joshua M. Spin, Ellen Kuhl and Philip S. Tsao

Circulation. 2015;131:1783-1795; originally published online April 22, 2015;
doi: 10.1161/CIRCULATIONAHA.114.012377
Circulation is published by the American Heart Association, 7272 Greenville Avenue, Dallas, TX 75231

Print ISSN: 0009-7322. Online ISSN: 1524-4539